ISSN 0036-0236, Russian Journal of Inorganic Chemistry, 2018, Vol. 63, No. 14, pp. 1772–1795. © Pleiades Publishing, Ltd., 2018.

ZrB_2/HfB_2–SiC Ultra-High-Temperature Ceramic Materials Modified by Carbon Components: The Review

E. P. Simonenko[a], *, N. P. Simonenko[a], V. G. Sevastyanov[a], and N. T. Kuznetsov[a]

[a]*Kurnakov Institute of General and Inorganic Chemistry, Russian Academy of Sciences, Moscow, 119991 Russia*

**e-mail: ep_simonenko@mail.ru*

Received June 8, 2018

Abstract—The review has been made of recent publications on modification of ZrB_2/HfB_2–SiC ultra-high-temperature ceramic composite materials (UHTC) by carbon components: amorphous carbon, graphite, graphene, fibers, and nanotubes. Available data have been presented on some aspects of oxidation of such materials at temperatures ≥1500°C and both at the atmospheric pressure and at the reduced oxygen partial pressure; structural features of the formed multilayer oxidized regions have been noted. It has been considered how the type and content of the carbon component and the conditions (first of all, temperature) of UHTC production affect the density, flexural strength, hardness, fracture toughness, and thermal and oxidation resistance of the modified ceramic composites.

Keywords: ultra-high temperature ceramic, composite, graphite, carbon fibers, carbon nanotubes, graphene, strength, fracture toughness, oxidation resistance

DOI: 10.1134/S003602361814005X

INTRODUCTION

The ceramic composite materials based on zirconium or hafnium diboride have high melting points (ZrB_2: 3040 ± 100°C [1], 3247 ± 18 [2]; HfB_2: 3250 ± 100°C [1], 3377°C [3]), high phase stability over a wide temperature range [1–5], high thermal conductivity (ZrB_2: 58.0 (300 K), 64.5 (1300 K), 134.0 (2300 K) [6]; HfB_2: 51.0 (300 K), 60.0 (1300 K), 143.0 (2300 K) [6]) (also at high temperatures), sufficiently high emissivity, and also high chemical and oxidation resistance. Owing to such properties, since approximately the 1960s [1, 6–8], these materials have generated considerable interest as promising for high-temperature service.

Modification of their composition by introducing silicon-containing high-melting compounds, first of all, silicon carbide, extends the range of possible applications also to oxygen-containing media [9–15]—as materials for the most critical parts of high-speed vehicles, propulsion systems, liners, etc. The preservation of high thermal conductivity of ZrB_2/HfB_2–SiC ceramics after adding 20–30 vol % silicon carbide enables one to regard these materials as candidates for sharp edges and nose parts (with a radius of curvature from fractions of a millimeter to several millimeters) of hypersonic vehicles. For this reason parts with sharp edges subjected to stagnation point aerodynamic heating are impacted by a high (several MW/m^2) heat flux, which results in an increase in the surface temperature above 2000°C [16–21]. However, ZrB_2/HfB_2–SiC ceramic composites do not fail by thermal shock owing to their ability to transmit heat through themselves and releases it from the system by radiation from relatively cool surfaces [22].

The number of systematic studies of the creation and modification of ultra-high-temperature ceramic composites and the determination of their properties increases year after year; more and more teams in various countries are involved in research on this subject. Figure 1 presents the results of the search on this subject, classified by countries of origin of authors. As is seen, most (~55%) works were published by Chinese authors; however, this search covered not only ceramics research but also studies of ceramic coatings based on super-refractory metal carbides and borides on the surface of C_f/C composites. Note that, from year to year, the range of countries in which studies on this subject are performed widens, and also new research teams form and develop, in the Russian Federation, too [23–32].

Despite a successful combination of the properties of the components, zirconium or hafnium diboride and silicon carbide, which brought ceramic materials based on them to the forefront of ultra-high-temperature applications, these materials have a number of drawbacks characteristic of most ceramics. First, this is low fracture toughness and insufficiently high resis-

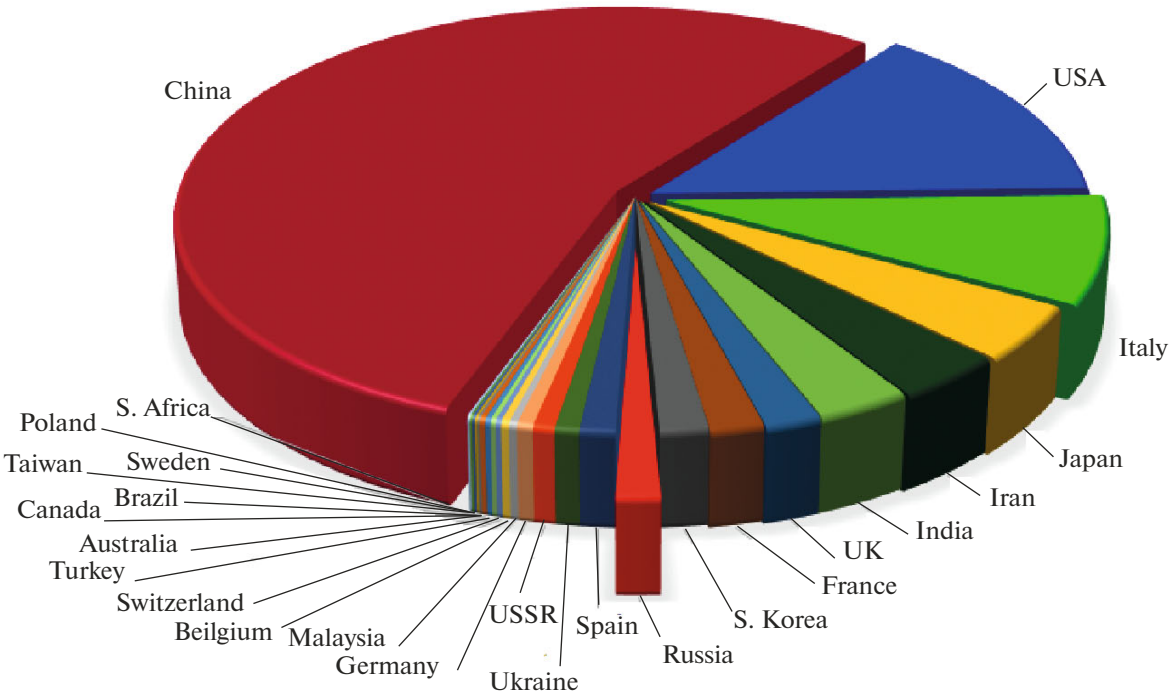

Fig. 1. Distribution of publications on ultra-high-temperature materials based on zirconium or hafnium diboride over countries of origin of authors, SciFinder, STN International, 02.2018.

tance to cyclic thermal shocks. Besides, because of low self-diffusion and strong covalent bonds in the crystal lattice of ZrB_2 and HfB_2, to produce UHTC with high enough density, high temperatures of hot pressing or sintering have to be used. This leads to significant growth of MB_2 grains (where M = Zr, Hf) and, hence, to impairment of mechanical properties. Thus, there is a compelling need to maximally reduce the temperature of production of ZrB_2/HfB_2–SiC ceramic materials.

The described adverse properties and processes are proposed to be overwhelmed or maximally neutralized by introducing modifying components to UHTC, in particular, carbon materials of various types.

This work is the review of the obtained data on modification of ZrB_2/HfB_2–SiC ultra-high-temperature ceramic composites by carbon components: carbon black, graphite, short carbon fibers, nanotubes, and graphene.

Fascinating technologies for creating functionally gradient materials based on continuous carbon fibers of the type of C_f/C and C_f/SiC composites the surface layer of which is modified by ZrB_2 and HfB_2, for forming laminated structures [33–37], and for applying protective antioxidation coatings to carbon materials are beyond the scope of this review.

1. FEATURES OF THE OXIDATION OF ZrB_2/HfB_2–SiC CERAMIC MATERIALS MODIFIED BY THE CARBON MATERIALS

Specific features and thermodynamic aspects of the oxidation of the ZrB_2/HfB_2–SiC UHTC and the causes of the formation of a SiC-depleted region by this oxidation were described in detail in the well-known works, which have already became classic [38–45].

In considering the problem of the modification of ceramic materials to be used at high temperatures (also above 2000°C) in an oxygen-containing atmosphere (also in the presence of atomic oxygen) by such a readily oxidizable substance as carbon, the idea immediately suggests itself that these materials should become less resistant to oxidation. Particularities of the oxidation of the MB_2–SiC–C materials that make it possible to characterize the materials within the general concepts of the behavior of materials of this type in the interaction with oxygen are most convincingly and analytically considered by Rezaie et al. [46], Jin et al. [47], and Nguyen et al. [48].

For example, Rezaie et al. [46] described the oxidation of ZrB_2–15 vol % SiC–15 vol % C (graphite) ceramic material, which was produced by hot pressing at 1950°C for 45 min under an uniaxial load of 32 MPa ($\rho_{rev} > 98\%$), in an air flow (p = 1 atm) at 1500°C to

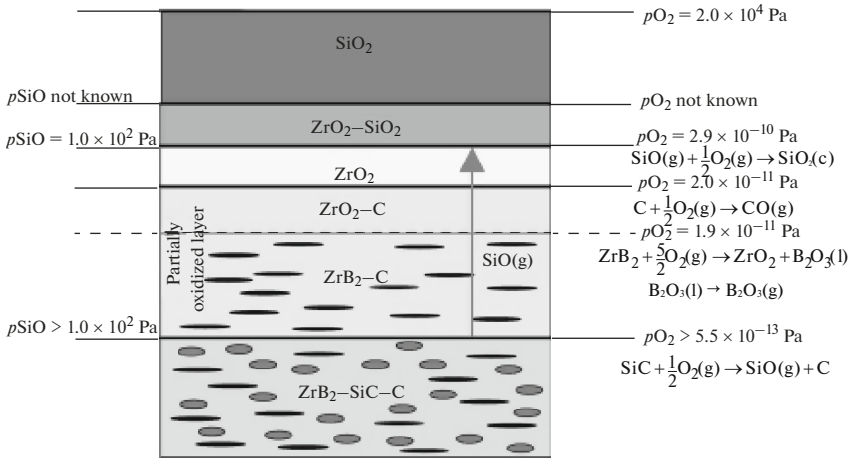

Fig. 2. Model of the distribution of layers in the structure formed by the oxidation of ZrB_2–15 vol % SiC–15 vol % C (graphite) ceramic composites in air at 1500°C [46].

form a layered structure. It was found that the pressing oriented graphite in the direction perpendicular to the pressing axis. The layer-by-layer determination of the phase composition in the oxidized region was performed by grinding away upper layers under the control of an optical microscope. It was shown [46] that the 8-h oxidation gave rise to a multilayer oxidized region the structure of which was more complex than those inherent in ZrB_2–SiC ceramic materials and comprised the following layers: upper amorphous layer 1 enriched with silicon dioxide, a protective borosilicate glass layer; thin layer 2 where ZrO_2 and SiO_2 coexisted, which passed into layer 3 consisting of the only crystalline ZrO_2; porous layer 4 based on ZrO_2, which contained graphite depleted with SiC, probably, by the active oxidation by the reaction (1) (under oxygen deficient conditions, graphite could also form from SiC by the reaction (2)); porous layer 5 based on ZrB_2 and graphite; and depleted SiC passing into the unoxidized material.

$$SiC + O_2 = SiO + CO, \quad (1)$$

$$SiC + O_2 = SiO_2 + C. \quad (2)$$

The calculated diagrams of oxidation at various oxygen pressures (volatility diagrams) at 1500°C for individual components of the system (ZrB_2, SiC, C) were combined into a single diagram and were used to determine the boundaries of the existence of these substances and the products of their oxidation at various total pressures and oxygen partial pressures.

By a combined analysis of the experimental data and the results of thermodynamic modeling, the model of distribution of layers of various compositions was constructed [46] (Fig. 2). As one can see, at this temperature, the oxygen pressure required for the active oxidation of the silicon carbide is $>5.5 \times 10^{-13}$ Pa. At the higher pressure of $pO_2 = 1.9 \times 10^{-11}$ Pa, ZrB_2 begins to be oxidized and after a further increase in the oxygen pressure to 2.0×10^{-11} Pa, the oxidation of graphite also begins.

Thus, Rezaie et al. [46] showed that the introduction of graphite leads not to inhibition of the active oxidation of silicon carbide, but to an almost twofold increase in the thickness of the partially oxidized layer.

Jin et al. [47] investigated the oxidation of ZrB_2–20 vol % SiC–15 vol % C (graphite) ceramic material at the higher temperature of 1800°C and reduced pressure: pO_2 in the chamber was 500 and 1500 Pa; the holding time in various experiments was 10, 30, 60, and 90 min. The total pressure in the system was 15 kPa, and the oxygen partial pressure was produced by mixing with argon. Samples were obtained by hot pressing at 1900°C for 1 h at a load of 30 MPa in an argon atmosphere ($\rho_{rel} > 99\%$).

According to the X-ray powder diffraction data [47], after the oxidation of samples for 10 min at oxygen partial pressures of both 500 and 1500 Pa, the dominant phase on the surface was tetragonal ZrO_2 with a small admixture of the monoclinic modification. Besides, there was also a ZrB phase, which was likely to form by the oxidation of ZrB_2 under oxygen deficient conditions by the reaction (3); the ZrB content of the samples oxidized at $pO_2 = 1500$ Pa was much lower. With increasing experiment duration, the content of the monoclinic phase ZrO_2 increased because, in the course of the oxidation, the particle

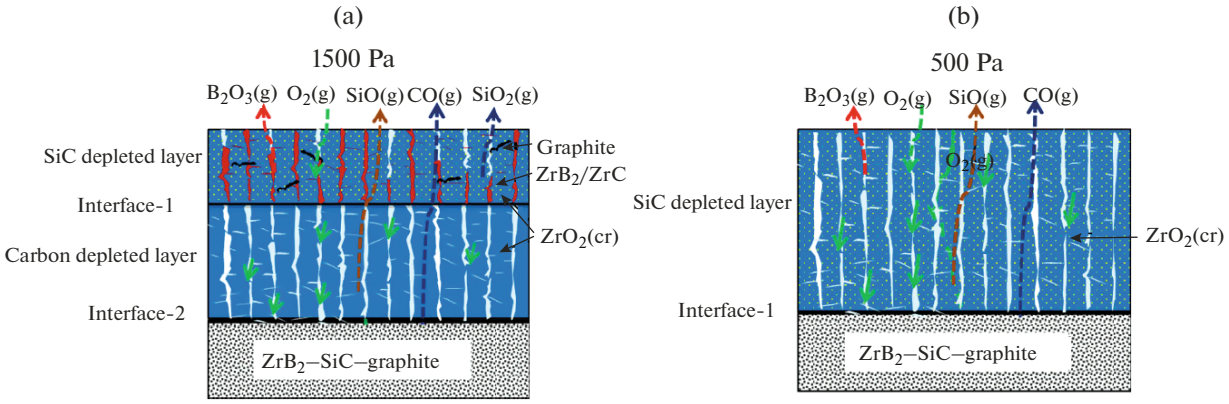

Fig. 3. Scheme of arrangement of oxidized layers and processes in the oxidation of ZrB_2–SiC–graphite samples at 1800°C and pO_2 = (a) 1500 and (b) 500 Pa [47].

size of t-ZrO_2 increased and t-ZrO_2 transformed to m-ZrO_2.

$$2ZrB_2(s) + 3/2O_2(g) = 2ZrB(s) + B_2O_3(l). \quad (3)$$

The X-ray photoelectron spectra showed [47] that, in all the samples, SiC on the surface was completely or partially (to SiO_xC_y) oxidized. The scanning electron microscopy images of polished samples together with the data of energy-dispersive X-ray spectroscopy and the X-ray photoelectron spectroscopy suggested that, by the oxidation at the higher oxygen pressure of 1500 Pa, a bilayer oxidized system formed. On the surface, there was a SiC-depleted layer, in which unoxidized graphite and traces of ZrC were found. Jin et al. [47] explained this by the fact that, in this case, because more ZrB_2 was oxidized to form ZrO_2, there was t-$ZrO_2 \rightarrow m$-ZrO_2 transition accompanied by an increase in the volume, which complicated the oxygen diffusion to the lower layer. At a greater depth, there is a layer depleted also with graphite. On the samples oxidized at pO_2 = 500 Pa, the only a silicon-depleted region formed, which was dominated by ZrO_2 passing directly into the unoxidized material [47] (Fig. 3).

Having analyzed the structure of the oxidized layer and the data on the kinetics of the increase of its thickness, Jin et al. [47] declared that they detected a transition at the temperature of 1800°C from the passive to the active mechanism of the surface oxidation of SiC (pO_2 < 1500 Pa). It was also noted that the addition of graphite to ZrB_2–SiC does not inhibit the formation of the oxidized layer (after the 10 min oxidation, the thicknesses of the oxidized layers on both composites are equal), but the oxidation rate for ZrB_2–SiC–C material is lower and is determined by the reaction rate, rather than by the oxygen diffusion rate.

Nguyen et al. [48] considered the oxidation of the ZrB_2–SiC, HfB_2–20 vol % SiC, and the ZrB_2–14 vol % SiC–30 vol % C ceramic materials in the water vapor medium. The oxidation was carried out at temperatures of 1200, 1300, and 1400°C in a 90% water vapor–10% oxygen flow in cyclic mode (10 cycles): 1 h in hot zone–20 min in cold zone. It was observed that, in the carbon-modified sample oxidized at any of the three temperatures, the main phase was $ZrSiO_4$, whereas in two the other samples, zirconium hafnium silicate occurred only as an admixture at an oxidation temperature of 1200°C, and the main phase on the surface was the corresponding oxide. The ZrB_2–14 vol % SiC–30 vol % C sample demonstrated the worst oxidation behavior: in this sample, the oxidized layer thickness was the largest, and so was the weight gain due to the oxidation of ZrB_2 and SiC. Nguyen et al. [48] noted that the studied materials cannot be used for a long time in aircraft engines because of their rapid degradation under combustion conditions.

Thus, the data of the few considered articles with a special focus on the oxidation mechanism suggested that the introduction of carbon to the ZrB_2/HfB_2–SiC UHTC does not make it necessary to totally revise the concepts of the interaction of these materials with oxygen. In the case of the oxidation at atmospheric pressure and temperatures of 1500–1700°C (where there is a protective borosilicate glass layer on the surface), one should perhaps expect an increase in the thickness of the SiC-depleted layer. In the oxidation at elevated temperatures (≥1800°C, at which glass evaporates from the surface of the samples) and reduced oxygen pressure, a transition to the active oxidation of silicon carbide on the surface, too, is quite probable, and graphite in this case may be more resistant to the interaction with oxygen.

2. EFFECT OF THE TYPE AND THE CONTENT OF CARBON MATERIALS AND THE CONDITIONS OF PRODUCTION OF ULTRA-HIGH-TEMPERATURE CERAMIC MATERIALS ON THEIR PROPERTIES

The introduction of carbon components to the ZrB_2/HfB_2–SiC ultra-high-temperature ceramic composites should certainly have some effect on their mechanical properties because, on the one hand, there is every prerequisite for improving the densification, and on the other hand, the addition of a the second phase of low strength should decrease this parameter and increase the fracture toughness.

The dispersity and morphology of the modifying carbon material should significantly affect the mechanical characteristics and the thermal shock resistance of the entire synthesized ceramics.

In this section, we separately considered the modification of ultra-high-temperature materials by amorphous carbon black, graphite, graphene, short fibers, and multilayer nanotubes.

2.1. Modification by Amorphous Carbon Black

At the beginning of our consideration, we analyzed several works in which amorphous carbon emerges in UHTC as a result of the pyrolysis of various carbon materials. For example, Zhou et al. [49] studied some mechanical properties and oxidation resistance of ZrB_2–20 vol % SiC–C samples obtained by pressureless sintering. For this purpose, ZrB_2 and SiC powders and a solution of phenolic resin were shredded in acetone, dried in air, and cold-pressed. The produced samples were carbonized at 800°C in vacuum and then sintered in argon at 2100°C for 2 h. It was noted that the presence of a certain amount of carbon led to an increase in the density from 93 to 98% and also to an insignificant increase in the flexural strength from 267.7 to 297.3 MPa (probably, owing to a decrease in porosity) and fracture toughness (K_{IC} increased from 3.13 to 3.68 MPa $m^{1/2}$.

Zhang et al. [50] introduced carbon to ceramic materials also by the pyrolysis of phenolic resin in producing ZrB_2–20 vol % SiC–3 wt % C–0.5 wt B_4C by pressureless sintering. The powders after drying were subjected to stepwise cold pressing (60 MPa → 200 MPa) with subsequent carbonization at 900°C for 1 h and sintering at 2100°C in an argon atmosphere. The authors [50] indicated (Table 1) that the density of the samples was 99.8%, the flexural strength was 361 ± 44 MPa (which on heating to 1200°C decreased only insignificantly to ~280 MPa), the hardness was 14.7 GPa, and the fracture toughness was 4.0 MPa $m^{1/2}$. The high thermal conductivity of the material (94 W m^{-1} K^{-1} at room temperature) with increasing temperature to 1200°C somewhat decreased to ~63 W m^{-1} K^{-1}. Zhang et al. [50] emphasized a high ablation resistance (oxyacetylene torch, first cycle at 2000°C for 180 s, second cycle at 2600°C for 300 s) and oxidation resistance on holding in stagnant air at 1400–1600°C for 30 min.

Zhou et al. [51] determined that the ZrB_2–xSiC ceramic materials (where x = 0, 5, and 16 vol %) produced by the pyrolysis of polycarbosilane on the surface of the ZrB_2 powder with subsequent hot pressing also contained amorphous carbon. However, the absence of accurate data on the composition, as well as the variation of the SiC content and the density simultaneously with the graphite content, prevents one from drawing a correct conclusion on the effect of carbon on the characteristics of the obtained UHTC samples.

Zhou et al. [52], Sun et al. [53], and Guo et al. [54] investigated the effect exerted on the mechanical properties of ceramic materials by carbon black—nanosized particles in the form of porous and compressible aggregates. Zhou et al. [52] the synthesized ZrB_2–20 vol % SiC–5 vol % C samples by hot pressing at 1900°C for 1 h and a load of 30 MPa with the addition of carbon black with an average particle size of 40 nm. For them, the density above 100% of the theoretical density was detected, which is explained by the formation of ZrC by the interaction of carbon with ZrO_2 impurities on the surface of ZrB_2 particles. The presence of zirconium carbide was confirmed by the X-ray powder diffraction analysis. The fact that, according to scanning electron microscopy data, ZrC was primarily concentrated at the ZrB_2 grain boundaries was confirmed by the origin of ZrO_2 in the samples. The modification of UHTC by nanosized carbon led to an increase in K_{IC} by 25% from 5.3 to 6.6 MPa $m^{1/2}$ and a simultaneous decrease in σ_f by 22% from 823 to 641 MPa. The fact that the thermal conductivity of the samples containing 5 vol % amorphous carbon was observed to be much higher than that of the unmodified sample throughout temperature range from room temperature (~100 W m^{-1} K^{-1}) to 1400°C (~50 W m^{-1} K^{-1}) was explained [52] by the removal of low-thermal-conductivity zirconium oxide from the ZrB_2 grain boundaries in the carbothermal synthesis of ZrC. Worthy of separate attention is a significant increase in the thermal shock resistance of the material, which was detected by determining the residual flexural strength after heating the samples to given temperatures (T = 200–1000°C) with subsequent quenching in water: at ΔT less than 600°C, σ_f changed insignificantly, and an abrupt decrease in the strength was observed only at ΔT = 800°C. As a the result, ΔT_c ($0.7\sigma_f$ at RT) increased by almost 80% from 395 to 705°C.

Table 1. Mechanical characteristics of MB_2–SiC–C ultra-high-temperature ceramic composites obtained under various conditions: relative density ρ_{rel}, flexural strength σ_f, Vickers hardness H_V, and fracture toughness K_{IC}

Composition, vol %	Production conditions	ρ_{rel}, %	σ_f, MPa	H_V, GPa	K_{IC}, MPa $m^{1/2}$	Ref.
Amorphous carbon						
ZrB_2–20SiC–13C–1.5B_4C	Pressureless sintering, 2100°C, 2 h, Ar	99.3	361 ± 44	14.7 ± 0.2	4.0 ± 0.5	[50]
ZrB_2–20SiC–5C	Hot pressing, 1900°C, 1 h, 30 MPa, Ar	99.2	641 ± 65	12.3 ± 1.1	6.6 ± 0.50	[52]
ZrB_2–20SiC–5C	Hot pressing, 1900°C, 1 h, 30 MPa, Ar	99.3	415.5	n/d[1]	6.5	[53]
ZrB_2–20SiC–10C		99.9	695.5		5.6	
ZrB2–20SiC–15C		98.3	499.9		4.7	
ZrB_2–20SiC–20C		92.3	265.9		3.2	
ZrB_2–20SiC–5C	Hot pressing, 2000°C, 1 h, 30 MPa, Ar	n/d[1]	n/d[1]	16.6 ± 0.3	7.52 ± 0.19	[54]
ZrB2–20SiC–10C				15.5 ± 0.2	7.17 ± 0.10	
Graphite						
ZrB_2–20SiC–10C	Hot pressing, 1900°C, 1 h, 30 MPa, Ar	99.7	490.8 ± 21.1	10.7 ± 0.9	6.1 ± 0.4	[55]
ZrB_2–20SiC–10C	Hot pressing, 1900°C, 1 h, 30 MPa, vacuum	99.7	490.8 ± 21.1	n/d[1]	6.06 ± 0.21	[56]
ZrB_2–20SiC–15C	Hot pressing, 2000°C, 1 h, 30 MPa, vacuum	100.2	481.0 ± 28.2	n/d[1]	6.11 ± 0.24	
ZrB_2–20SiC–20C		98.1	367.8 ± 20.2	n/d[1]	5.21 ± 0.18	
ZrB_2–20SiC–30C		97.2	277.1 ± 10.2	n/d[1]	4.07 ± 0.15	
ZrB_2–20SiC–10C	Hot pressing, 1850°C, 1 h, 20 MPa, vacuum	99.6	n/d[1]	16.5 ± 0.9	7.1 ± 0.5	[59]
ZrB_2–20SiC–10SiC_W–10C	Hot pressing, 1800°C, 1 h, 30 MPa, Ar	99.6	600 ± 75	n/d[1]	6.4 ± 0.6	[60]
ZrB_2–20SiC–15C	Hot pressing, 1900°C, 1 h, 30 MPa, Ar	n/d[1]	480 ± 22	n/d[1]	6.1 ± 0.25	[61]
ZrB_2–20SiC–15C⊥	Hot pressing, 1900°C, 1 h, 30 MPa, vacuum	n/d[1]	481.0 ± 25.2	11.2 ± 0.5	6.11 ± 0.25	[62]
ZrB_2–20SiC–15C‖		n/d[1]	387.2 ± 19.1	10.8 ± 1.2	4.30 ± 0.15	
ZrB_2–20SiC–15C	Hot pressing, 1900°C, 1 h, 30 MPa, Ar	99.6	498.8	n/d[1]	6.11	[64]
ZrB_2–20SiC–15C	Hot pressing, 1900°C, 1 h, 30 MPa, Ar	n/d[1]	478 ± 24	n/d[1]	6.1 ± 0.3	[67]
ZrB_2–20SiC–15C	Hot pressing, 1800°C, 1 h, 30 MPa, Ar	99	396		4.90	[72]

Table 1. (Contd.)

Composition, vol %	Production conditions	ρ_{rel}, %	σ_f, MPa	H_V, GPa	K_{IC}, MPa $m^{1/2}$	Ref.
ZrB_2–25SiC–11C[2]	SPS, 1900°C, 7 min, 40 MPa, vacuum	100	n/d[1]	18	4.9	[74]
ZrB_2–25SiC–20C[2]		100.7		16	6.7	
ZrB_2–25SiC–27C[2]		99.7		15	8.2	
ZrB_2–25SiC–33C[2]		98.3		12.1	–	
ZrB_2–20SiC–15.5C[2]	SPS, 1950°C, 10 min, 100 deg/min, 38 MPa		318	n/d[1]	3.09	[76]
Graphene						
ZrB_2–25SiC–5 wt % C_G	Hot pressing, 1850°C, 1 h, 20 MPa, Ar	99.1	n/d[1]	15.7 ± 0.5	6.4 ± 0.4	[85]
ZrB_2–20SiC–C_G (2 vol % GO)	Hot pressing, 1950°C, 1 h, 30 MPa, Ar	98.9	698 ± 52	22.93 ± 1.83	6.07 ± 0.25	[86]
ZrB_2–20SiC–C_G (5 vol % GO)		99.2	1055 ± 64	22.76 ± 2.07	7.32 ± 0.37	
ZrB_2–20SiC_W–C_G (5 vol % GO)	Hot pressing, 1950°C, 1 h, 30 MPa, Ar	98.5	764	n/d[1]	6.6	[87]
ZrB_2–20SiC_W–C_G (10 vol % GO)		99.3	681		5.8	
ZrB_2–20SiC–0.5 wt % C_G (ZrB_2–20SiC–2.5C_G)[2]	SPS, 2000°C, 10 min, 30 MPa, 100 deg/min, Ar	n/d[1]	1050	n/d[1]	5.6	[88]
ZrB_2–20SiC–1 wt % C_G (ZrB_2–20SiC–4.5C_G)[2]			950		6.3	
ZrB_2–20SiC–2 wt % C_G (ZrB_2–20SiC–9.5C_G)[2]			940		6.93	
ZrB_2–20SiC–3 wt % C_G (ZrB_2–20SiC–13.5C_G)[2]			630		4.58	
Short carbon fibers						
ZrB_2–20SiC–20C_f	Hot pressing, 2000°C, 1 h, 30 MPa, Ar	99.3	445 ± 36	n/d[1]	6.56	[89]
ZrB_2–20SiC–20C_f	Hot pressing, 2000°C, 1 h, 30 MPa, Ar	98.5	397 ± 42	n/d[1]	6.35 ± 0.3	[90]
ZrB_2–20SiC–20C_f	Hot pressing, 2000°C, 1 h, 30 MPa, Ar	98	445 ± 36	n/d[1]	6.56 ± 0.	[91]
ZrB_2–20SiC–20C_f	Hot pressing, 2000°C, 1 h, 30 MPa, Ar	99.3	445 ± 36	19.2 ± 0.8	6.6 ± 0.1	[93]

Table 1. (Contd.)

Composition, vol %	Production conditions	ρ_{rel}, %	σ_f, MPa	H_V, GPa	K_{IC}, MPa $m^{1/2}$	Ref.
HfB_2–20SiC–20C_f	Hot pressing, 2100°C, 1 h, 20 MPa, Ar	99.5	n/d[1]	n/d[1]	5.6 ± 0.2	[94]
HfB_2–20SiC–30C_f		99.3			5.7 ± 0.3	
HfB_2–20SiC–40C_f		98.3			5.9 ± 0.3	
HfB_2–20SiC–50C_f		98.1			6.1 ± 0.2	
ZrB_2–20SiC–30C_f	SPS, 1900°C, 100 deg/min, 30 MPa	98.7	345 ± 54	n/d[1]	3.21 ± 0.12	[98]
ZrB_2–20SiC–30C_f	Hot pressing, 1600°C, 2 h, 30 MPa, Ar	95.8	335 ± 17		4.56 ± 0.13	
ZrB_2–20SiC–30C_f–PyC	Hot pressing, 1600°C, 2 h, 30 MPa, Ar	95.3	317 ± 12		6.16 ± 0.15	
ZrB_2–20SiC–30C_f	Hot pressing, 1450°C, 2 h, 30 MPa, Ar	95.8	341 ± 21	n/d[1]	6.12 ± 0.12	[99]
ZrB_2–20SiC–20C_f	Hot pressing, 1450°C, 2 h, 30 MPa, vacuum	98.2	375 ± 18	n/d[1]	5.20 ± 0.19	[100]
ZrB_2–20SiC–30C_f		97.1	325 ± 12		5.87 ± 0.17	
ZrB_2–20SiC–40C_f		85.7	154 ± 7		3.12 ± 0.10	
ZrB_2–20SiC–50C_f		80.4	98 ± 4		2.26 ± 0.05	
ZrB_2–20SiC–10C_f	SPS 1850°C, 6 min, 30 MPa	n/d[1]	n/d[1]	14.8	6.8	[102]
Carbon nanotubes						
ZrB_2–20SiC–2C_{CNT} (ZrB_2–20SiC–9.5C_{CNT})[2]	Hot pressing, 1900°C, 1 h, 30 MPa, Ar	n/d[1]	616 ± 97	15.5 ± 0.9	4.6 ± 0.6	[105]
ZrB_2–20SiC–10C_{CNT}	Hot pressing, 1850°C, 1 h, 20 MPa, Ar	93.9	n/d[1]	8.6 ± 0.3	5.1 ± 0.8	[106]
ZrB_2–20SiC–15C_{CNT}	SPS, 1600°C, 25 MPa, 10 min	94.6	472 ± 46	11.5 ± 0.7	5.9 ± 0.6	[107]
	SPS, 1650°C, 25 MPa, 10 min	96.2	485 ± 35	12.8 ± 0.5	7.1 ± 0.1	
	SPS, 1700°C, 25 MPa, 10 min	98.0	490 ± 43	13.0 ± 0.5	7.2 ± 0.3	
	SPS, 1750°C, 25 MPa, 10 min	99.1	565 ± 16	16.0 ± 0.6	8.0 ± 0.2	
	SPS, 1800°C, 25 MPa, 10 min	99.1	516 ± 33	15.5 ± 0.7	6.9 ± 0.5	
ZrB_2–20SiC–10C_{CNT}	SPS, 40 MPa, stepwise heating 1300 (5 min) → 1500 (5 min) → 1650°C (5 min), 150 deg/min, Ar	99.7	390.4 ± 3.9	n/d[1]	9.5 ± 0.8	[108]
ZrB_2–20SiC–10C_{CNT}		99.7	n/d[1]	21.0 ± 0.7	n/d[1]	[109]
37ZrB_2–37HfB_2–20SiC–6C_{CNT}	SPS, 1850°C, 10 min, 30 MPa, vacuum, 100 deg/min	99.5	n/d[1]	28.1 ± 1.2	10.2 ± 0.3	[110]

[1] Parameter was not determined or was not indicated in a reference.
[2] Conversion from wt % to vol % was performed by the authors of this review.

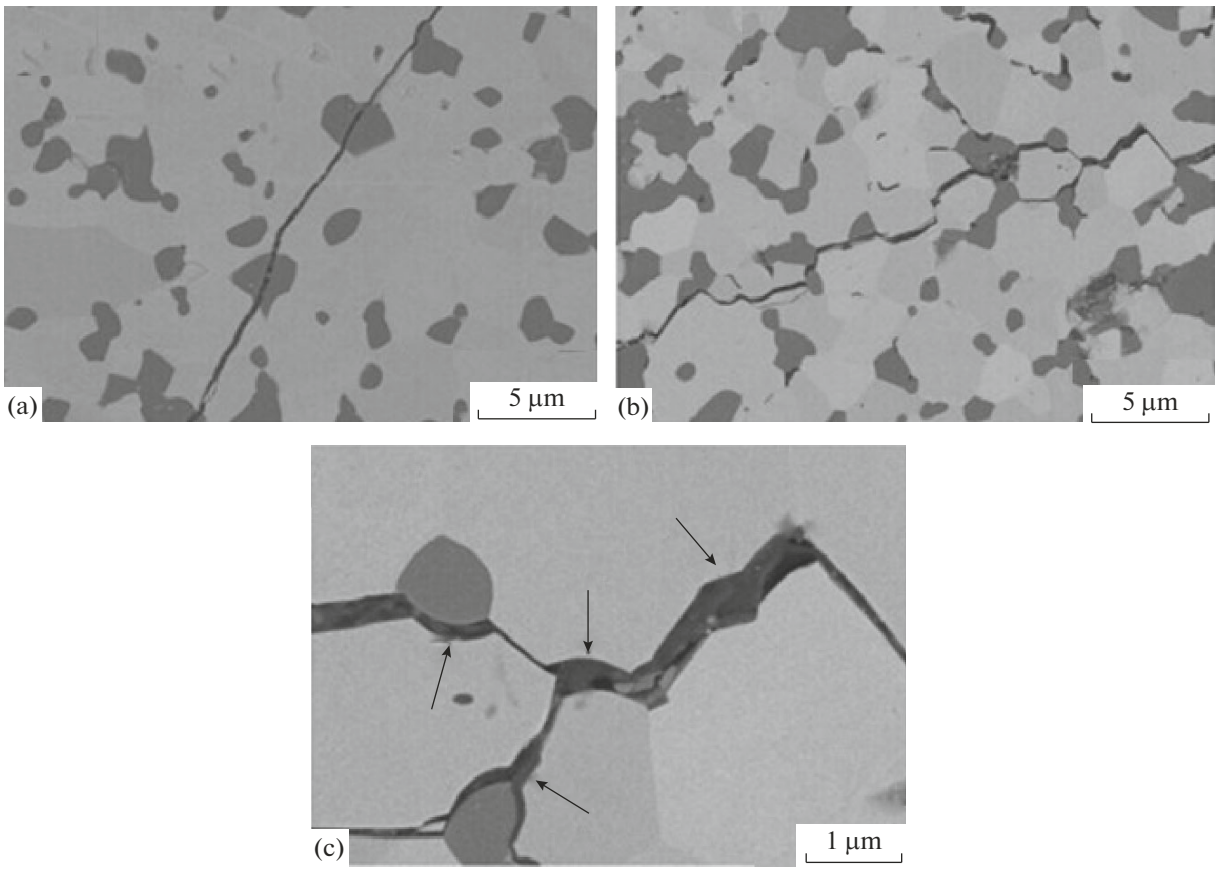

Fig. 4. Propagation of cracks produced by the indentation of a Vickers pyramid into (a) ZrB_2–20 vol % SiC and (b, c) ZrB_2–20 vol % SiC–5 vol % C samples [54].

Sun et al. [53] studied the effect of the content of carbon black (average particle size 200 nm) on the mechanical properties of synthesized ceramic materials. The ZrB_2–20 vol % SiC–(5, 10, 15, and 30) vol % C samples were produced as described above [52]. The maximum density (99.9%) and the maximum flexural strength (695.6 MPa) were observed for the samples containing 10 vol % SiC, and the maximum K_{IC} (6.5 MPa $m^{1/2}$) was detected in the samples containing 5 vol % SiC. It was determined that the addition of carbon to a content of above 15 vol % impairs the mechanical properties because of the aggregation of carbon black on grain boundaries.

Amorphous carbon nanospheres 100–200 nm in diameter were used for producing ZrB_2–20 vol % SiC–(0, 5, and 10) vol % C UHTC by hot pressing at 2000°C for 1 h at a load of 30 MPa. It was observed that, under these conditions, carbon graphitization begins: the X-ray powder diffraction patterns of the samples containing 10 vol % C had the corresponding reflections. With increasing carbon content, the hardness systematically decreased, and the fracture toughness somewhat increased: the maximum K_{IC} (7.52 MPa $m^{1/2}$) was reached at a carbon content of the ceramics of 5 vol %. The crack arrest during failure was primarily due to crack deflection and branching (Fig. 4) because carbon concentrated at grain boundaries weakened the intergrain interactions.

Thus, the addition of a small amount of amorphous carbon (to a content of 5–10 vol %) improves the sintering of UHTC and increases fracture toughness, which is accompanied by a certain decrease in flexural strength and hardness. The properties of produced ceramics are likely to strongly depend not only on the amount of the introduced amorphous carbon and the production conditions of the ceramics, but also on the uniformity of the carbon distribution in the bulk of the material and the dispersity of carbon, unfortunately, the available data are scarce and do not enable one to determine general regularities of the changes in the properties.

Note, however, that, because the carbon component is primarily distributed at grain boundaries and the temperature of the production of the ceramics are quite high, the samples are purified in situ so that the ZrO_2 and SiO_2 oxide impurities are removed. This was

considered [52] to be the cause of the observed increase in the thermal conductivity.

2.2. Modification by Graphite Micro- and Nanoflakes

The data on the modification of ZrB_2/HfB_2–SiC ultra-high-temperature ceramic materials by graphite particles shaped as flakes with a high diameter-to-thickness ratio are most abundant. Many researchers regard them as a substitute for SiC whiskers in the context of the possibility of increasing the fracture toughness of materials, including by bridging and also by the relaxation of stresses near the crack tip against the layered materials. It was these arguments, as well as the ability of graphite flakes to self-lubrication during compaction, that guided Zhang et al. [55] and other authors in choosing a modifying component for UHTC.

2.2.1. ZrB2–20 vol % SiC–10 vol % C, hot pressing. Zhang et al. [55] produced the ZrB_2–20 vol % SiC–10 vol % C ceramic materials with a density of 99.7% by hot pressing using graphite flakes 15 μm in diameter and 1.5 μm in thickness at 1900°C for 1 h at a uniaxial load of 30 MPa in argon. The X-ray powder diffraction analysis showed the presence of a ZrC impurity, which formed by the carbothermal reduction of ZrO_2 on the surface of ZrB_2 particles and was introduced by grinding by ZrO_2 balls. The flexural strength was 491 MPa, and the Vickers hardness was 10.7. The fact that the value K_{IC} = 6.1 MPa $m^{1/2}$ was elevated in comparison with that for the unmodified material was explained [55] by more complex mechanism of failure, in which there were both crack deflection and branching, and signs of stretching of graphite flakes.

Wang et al. [56] demonstrated that an increase in the content of graphite flakes in producing UHTC to 15 vol % under similar conditions of the synthesis of ceramics did not allow considerably increase the fracture toughness but caused a decrease in σ_f to 481 MPa. A simultaneous increase in the content of graphite flakes to 20 and 30 vol % and in the hot-pressing temperature to 2000°C led to a decrease both in the flexural strength (to 368 and 277 MPa, respectively) and in K_{IC} (to 5.21 and 4.07 MPa $m^{1/2}$), which was explained [56] by the fact that, in comparison with the ZrB_2–20 vol % SiC–(10, 15) vol % C samples, the samples containing 20 and 30 vol % C were characterized by higher (by 2–3%) porosity and the larger sizes of grains of the main phases. The thermal shock resistance described by the critical crack size in brittle failure systematically decreased with increasing carbon component content.

Jin et al. [57] studied the thermal resistance of the ZrB_2–20 vol % SiC–10 vol % C material obtained according to a similar procedure [55, 56]. In this study, the temperature difference was created not by quenching in water after heating but by rapid (4–11 s) electrical heating to a temperature at the center of the sample of 200–2000°C with subsequent cooling (4–7 s), with the heating rate being varied from 200 to 500 deg/min. The oxygen pressure in the chamber was maintained at pO_2 = 200 Pa. Jin et al. [57] showed that, at the minimum rate of heating to temperatures ≤1600°C, the residual σ_f systematically decreased to ~400 MPA, and within the range 1600–1800°C, the residual strength increased to 450–470 MPa, which was due to healing of defects on the surface during the formation of the borosilicate glass layer and to the generation of a compressive stress in the oxide layer. At a temperature >1800°C, the residual strength decreased to ~270 MPa. At the maximum heating rate, the residual strength did not increase: σ_f systematically decreased to 170 MPa (2000°C), probably, for lack of time for the formation of an oxidized layer on the surface of the ceramics.

In another work [58], Jin et al. obtained close results: the experiment was carried out over a wider temperature range (to 2500°C) at a heating rate of 300 deg/min. It was observed that, on heating to 2500°C, the samples failed.

Using graphite nanoparticles (average size 10–80 nm) [59] in hot pressing in vacuum at reduced temperature (1850°C) and reduced load (20 MPa) enabled one to produce ZrB_2–20 vol % SiC–10 vol % C samples with high hardness (H_v = 16.5 GPa) and high fracture toughness (7.1 MPa $m^{1/2}$). The average ZrB_2 grain size in the modified samples was half as large as that in the ZrB_2–20 vol % SiC materials (6.9 μm as against 3.2 μm). In the failure of the samples because of the introduction of nanosized graphite particles, there were crack deflection and branching, bridging, crack stress relaxation on the layered nanomaterial, and also pullout of graphite planes from grains of graphite nanoflakes.

Improvement of the mechanical properties was shown [60] to be promoted both by using ZrB_2 nanoparticles and by introducing the second, also nanosized, modifying component—SiC whiskers (to the final UHTC composition ZrB_2–20 vol % SiC–15 vol % C). It was determined that the flexural strength increased to 600 ± 75 MPa (which may be related to a partial load transfer to SiC whiskers), and the fracture toughness was 6.4 ± 0.6 MPa $m^{1/2}$.

2.2.2. ZrB_2–20 vol % SiC–15 vol % C, hot pressing. Wang et al. [61] investigated the effect of the content of graphite flakes in producing ZrB_2–20 vol % SiC–15 vol % C ceramic materials by hot pressing (1900°C, 1 h, 30 MPa, Ar) on the mechanical properties of the materials. By and large, the obtained data [61] agree with those considered above [56]: the flex-

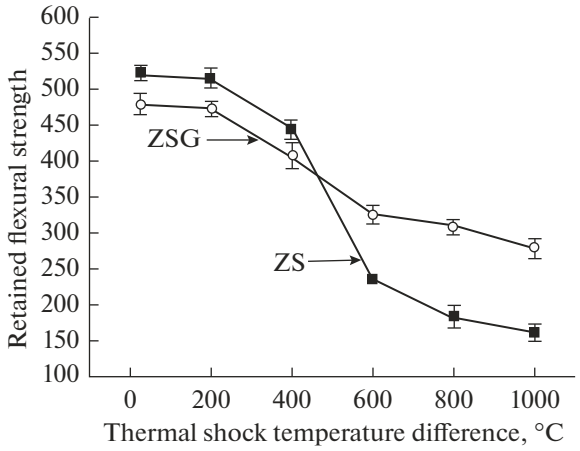

Fig. 5. Retained flexural strength after heating to an indicated temperature in air and quenching in water for samples ZrB_2–20 vol % SiC (ZS) and ZrB_2–20 vol % SiC–15 vol % C (ZSC) [61].

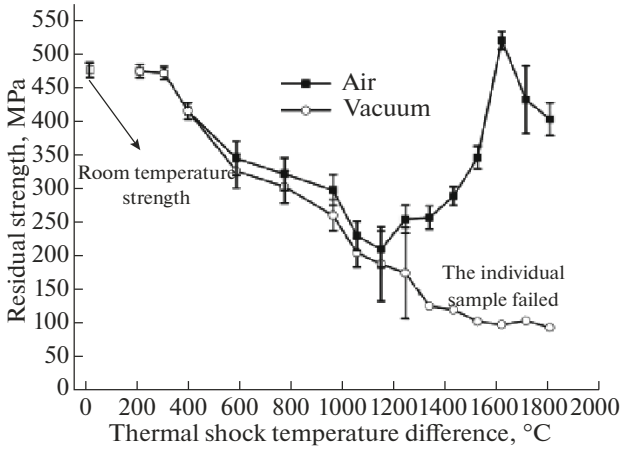

Fig. 6. Residual flexural strength after heating to an indicated temperature in air and in vacuum with subsequent quenching in water for the ZrB_2–20 vol % SiC–15 vol % C samples [63].

ural strength was 480 MPa (which was 8% lower than that for the unmodified material ZrB_2–20 vol % SiC), and the fracture toughness was 6.1 MPa $m^{1/2}$ (which was 30% higher than the value for ZrB_2–20 vol % SiC [61], but differed insignificantly from the value for ZrB_2–20 vol % SiC–10 vol % C [55, 56]). The increase in the thermal conductivity throughout the temperature range (30–1000°C), which was ensured by introducing the high-thermal-conductivity graphite particles, provided elevated thermal shock resistance in quenching of heated samples in water (Fig. 5). It was noted [61] that, as it was also inherent in the samples containing 10 vol % C, the hot pressing oriented graphite particles in the direction perpendicular to the pressing axis (which caused anisotropy of the properties), and at grain boundaries there were microcracks formed because of the difference in linear thermal expansion coefficient between the components of the ceramic.

Zhou et al. [62] showed that the difference in the mechanical properties because of the preferential orientation of graphite flakes in the bulk of UHTC was quite significant. For example, for the ZrB_2–20 vol % SiC–15 vol % C sample, the flexural strength in the direction perpendicular to the hot-pressing direction was 20% higher than that in the parallel direction (in which the material fails along the plane of graphite flakes), and the fracture toughness was 30% higher.

Hu et al. [63] discussed the thermal resistance in air and in vacuum for composites that contained 15 vol % graphite and were obtained similarly [55–57, 61, 62]. Generally, the results of measuring the residual strength after heating to a given temperatures and quenching agreed with the data obtained [57] on the ZrB_2–20 vol % SiC–10 vol % C sample: in a vacuum, the strength systematically decreased because of the generation of additional thermal stresses (and at $\Delta T >$ 1200°C, most of the samples failed), whereas in air the dependence was more complex (Fig. 6).

Hu et al. [63] demonstrated that, only on heating in air at the temperature of 1200°C and higher (to ~1700°C), SiC began to be oxidized to form the flaw-healing borosilicate glass on the surface. Increasing temperature improved the wettability of the surface of the material by liquid glass, which led to an increase in the residual strength to 530 MPa (1700°C), i.e., to a value that was even higher than the strength of the initial UHTC. At ΔT = 1800°C, ZrO_2 particles on the surface had still been fully coated with glass, but bubbles indicating active gas formation were already forming in the glass. At ΔT =1900°C on heating in air, on the surface, there was already primarily dense ZrO_2, the increase in the volume of which was considered [63] to be the cause of a certain sealing of the surface flaws and a relatively high flexural strength (~400 MPa). Thus, it was confirmed that the surface oxidation of ZrB_2–20 vol % SiC–15 vol % C ceramics can have a considerable effect on their mechanical properties.

Wang et al. [64] examined the change in the mechanical properties in the course of the surface oxidation at 1100°C in dry and wet air. It was found that, in these cases, the composition and the microstructure of the surface layer of the ceramic composite differed significantly. In the oxidation in dry air, on the surface, a continuous (or, after long-term holding for 60 and 90 min, cracked) glass layer based on primarily B_2O_3 formed (SiC at this temperature was oxidized insignificantly). After heating of the samples in wet air, the presence of a glass phase on the surface was insig-

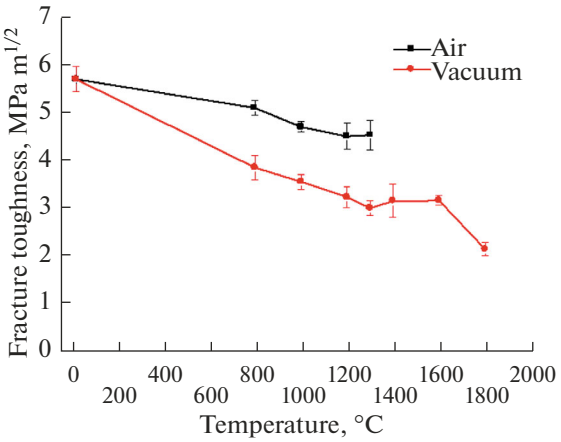

Fig. 7. Change in the fracture toughness of the ZrB_2–20 vol % SiC–15 vol % C samples after their 10-min heating in vacuum and in air [65].

nificant, and H_3BO_3 flakes primarily formed. It was shown that, although crack healing was more efficient in the oxidation of composites in dry air, the residual strength after introducing a defect in both cases increased from 371.7 to 469.9 (dry air) or 449.3 (wet air) MPa.

Specific features of the oxidation in vacuum and in air were considered [65] to explain different kinetics of the decrease in the high-temperature fracture toughness on heating samples to a given temperature and holding for 10 min (Fig. 7): in the latter case, K_{IC} was much higher. It was indicated [65] that the brittle-to-ductile transition temperature was ~1300°C.

Niu et al. [66] and Jin et al. [67] investigated the directed healing of cracks on the surface of UHTC samples obtained under the described conditions by the oxidation by the atomic oxygen at the low pressure (50 Pa, O_2 : Ar = 1 : 4). It was shown [66] that the residual strength after creating the defect in the form of the crack (194.5 MPa) increased to 218 (1400°C) and 260 MPa (1600°C), which was explained [66] by healing the crack owing to an increase in the volume because of the formation of zirconium dioxide by the oxidation and its phase transformation t-$ZrO_2 \rightarrow m$-ZrO_2, and also thanks to the filling of the crack tip with detached ZrO_2 particles driven by the liquid borosilicate glass.

Jin et al. [67] studied the changes in the mechanical properties of the material without specially creating a defect during the oxidation by the atomic oxygen at the pressure in the chamber of 50 Pa [67]. Both the strength and the fracture toughness decreased with increasing temperature to 1600°C (holding time 30 min) from 478 to 372 MPa and from 6.1 to 4.2 MPa m$^{1/2}$, respectively. The same trend was also observed with increasing holding time at the temperature of 1600°C from 5 to 90 min. Such behavior was explained [67] by an increase in the thickness of the porous oxidized layer based on ZrO_2; this layer was more prone to peel off from the unoxidized part of the material than in the case of the oxidation in air, when there was the borosilicate glass layer on the surface.

Wang et al. [68] studied the changes in the mechanical properties of the ceramic materials of the above composition as the result of their annealing at 1600–1800°C without load in argon in order to relax stresses generated by hot pressing of components with widely different thermal expansion coefficients. It was shown that, with increasing temperature and duration of heat treatment, the flexural strength increased from 480 to 577 MPa (1800°C, 60 min), and the fracture toughness decreased from 6.11 to 5.03 MPa m$^{1/2}$. At the same time, the Vickers hardness changed nonmonotonically: the maximum value was reached after heat treatment at 1700°C for 90 min.

Wang et al. [69], Zhang et al. [70], and Chen et al. [71] considered the results of measuring the tensile strength of hot-pressed UHTC containing 15 vol % graphite flakes. Wang et al. [69] measured the high-temperature strength within the range 1300–1800°C. It was found that, in comparison with the value σ = 134 MPa measured at room temperature, the strength at the temperature of 1800°C dropped to 60 MPa. Preoxidation of the surface at 1550–1750°C for 10 min [70] led to a systematic decrease in the strength from 118.2 to 21.8 MPa. Chen et al. [71] demonstrated that preloading of samples with tensile stress (30–60 MPa) led to a significant decrease in the number of cycles of heating to the temperatures of 1900 and 2500°C until failure of the material.

Decreasing temperature of hot pressing of the ZrB_2–20 vol % SiC–15 vol % C ceramics to 1800°C was reported [72] to lead to lower values of the flexural

strength (σ_f = 396 MPa) and the fracture toughness (K_{IC} = 4.90 MPa $m^{1/2}$).

2.2.3. Spark plasma sintering. Works about spark plasma sintering (SPS) synthesis of UHTC modified by graphite flakes are much fewer than those on using hot pressing. In the earliest work [73], for improving spark plasma sintering of ZrB_2–30 vol % SiC at 1750°C, graphite to the content of 2 wt % (~8.8 vol %) was added; the compacting kinetics was improved, but it was noted that, by this method, oxide impurities cannot be removed from the surface of ZrB_2 and SiC particles.

Shahedi Asl et al. [74] studied the effect of the content of the added nanosized graphite component in ZrB_2–25 vol % SiC–(0, 2.5, 5, 7.5, 10) wt % C materials in SPS in vacuum at 1900°C for 7 min at a load of 40 MPa. It was determined that, because of carbothermal processes involving oxide impurities, on the surface of ZrB_2 and SiC particles in samples containing 5 wt % (~20 vol %) carbon, a density of 100.7% was observed (the X-ray powder diffraction patterns showed reflections of ZrC and B_4C). With increasing content of the graphite component in UHTC, there were a systematic decrease in the ZrB_2 grain size in the ceramics and a decrease in the hardness from 19.5 (0% C) to 12.1 GPa (10 wt % C) and in Young's module from 478 (0% C) to 385 GPa (10 wt % C). The fracture toughness increased from 4.3 (0% C) to 8.2 MPa $m^{1/2}$ (~7.5 wt % C). Along with crack deflection and branching, crack bridging by graphite flakes and pullout of graphite planes were also observed.

To reach the maximum densification of UHTC, Shahedi Asl [75] performed the Taguchi analysis to optimize such process parameters as the composition of ZrB_2–25 vol % SiC–(0, 2.5, 5, 7.5, 10) wt % C ceramic composite, temperature, holding time, and load in SPS. Shahedi Asl [75] established that the maximum contribution to the densification was made by an increase in the SPS temperature and the graphite content. The following parameter values were chosen to be optimum: the maximum studied SPS temperature (1900°C), the maximum SPS load (40 MPa), the holding time 7 min, and the graphite nanoflake content 5 wt % (20 vol %).

Somewhat aside is Cheng et al.'s work [76], in which spark plasma sintering was applied to the ZrB_2–SiC–C composite nanopowders synthesized by the sol–gel method. Note that the sol–gel synthesis of the ZrB_2/HfB_2–SiC–C composite nanopowders for producing UHTC based on them is a highly promising and actively developed research area [77–80]. In recent works [81–84], the ceramic materials were produced by hot pressing or spark plasma sintering of the MB_2–(SiO_2–C) composite powders synthesized by the sol–gel method, and the oxidation of these materials in sub- and supersonic dissociated air flows were studied. In general, this method has a lot of advantages; first of all, it enables one to obtain the nanostructured powders the components of which are maximally uniformly distributed in each other.

In Cheng et al.'s work [76], in mixing precursors ($Zr(OPr^i)_4$, $Si(OC_2H_5)_4$, H_3BO_3, and $C_6H_{14}O_6$ (sorbitol)), an excess of the organic component was intentionally used, which made it possible, after gel formation, drying, and carbothermal synthesis, to obtain the ZrB_2–20 vol % SiC–3.5 wt % C composite powder. Noteworthily, before spark plasma sintering at 1950°C (10 min, 100 deg/min) and 38 MPa, the carbon phase was the X-ray amorphous, whereas in UHTC, according to the Raman spectroscopy and X-ray powder diffraction data, graphite layers formed. Probably, because of the fact that, directly at SPS, the carbon component was, in substance, carbon black, and its content was high enough (~15.5 vol %), the measured values of the flexural strength and the fracture toughness were moderate 318 MPa and 3.08 MPa $m^{1/2}$, respectively.

Analyzing the data of Table 1, which summarizes the existing information on mechanical properties of UHTC modified by graphite flakes, one can conclude that using nanoparticles improves the mechanical properties, probably, both by increasing the length of grain-boundary cracks and by ensuring more uniform distribution of components in the bulk of the material. A certain additional increase in the fracture toughness by modification by graphite flakes in comparison with the case of addition of amorphous carbon may be due to the emergence of additional mechanisms of crack arrest, which are possible owing to the layered structure of graphite—bridging and pullout of graphite planes.

2.3. Modification by Graphene

The transition from modification by graphite flakes to modification by graphene is locical and practical because graphene has all the advantages of graphite layers and, on top of all, still higher ratio of the diameter of a particle to its thickness, which increases the toughening efficiency. For example, Yang et al. [85] modified the ZrB_2–25 vol % SiC ceramic material by adding 5 wt % graphene with an average particle diameter of 4–12 μm and an average particle thickness of 2–18 nm. A graphene powder was ultrasonically dispersed in ethanol, and to the obtained dispersion, ZrB_2 and SiC powders were added. After drying, grinding, and hot pressing at 1850°C (1 h) and 20 MPa, the ceramic material was produced, which has a density of 99.1% and elevated (in comparison with the unre-

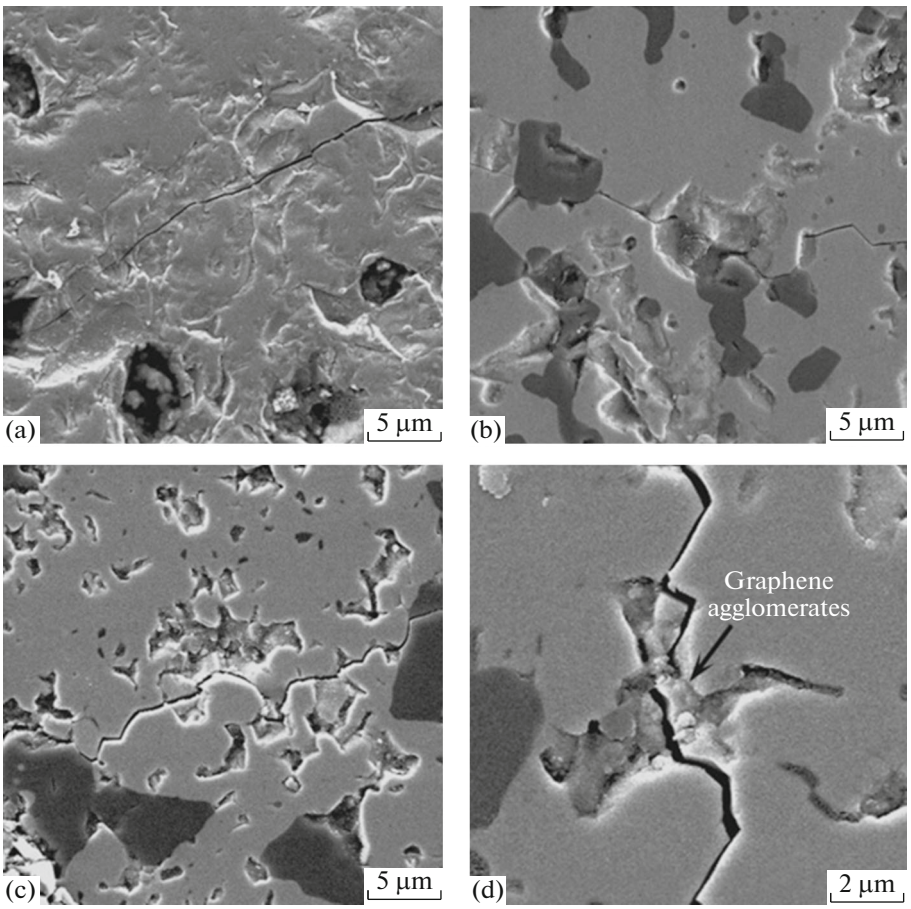

Fig. 8. Crack propagation in (a) ZrB_2, (b) ZrB_2–SiC, and (c, d) ZrB_2–SiC–C_G ceramics [85].

inforced material) values of the hardness (15.7 ± 0.5 GPa, Table 1) and the fracture toughness (K_{IC} = 6.4 MPa $m^{1/2}$). Yang et al. [85] noted that the toughening was due to crack deflection (including at the boundaries of graphene flakes (Fig. 8)), crack branching, and pull-out of graphene flakes. It was also detected that graphene particles in the produced ceramics were highly agglomerated.

To mitigate the problem of agglomeration of graphene particles, the ZrB_2–20 vol % SiC ultra-high-temperature composite was modified [86] by graphene oxide (GO), which is well stabilized in ethanol and readily reducible to graphene on heating in vacuum to 1100°C. To a GO dispersion, ZrB_2 and SiC powders were added in ratios necessary for obtaining materials containing 2 and 5 vol % graphene oxide. Hot pressing in argon at 1950°C for 1 h at a load of 30 MPa gave samples with densities of 98.9 (2 vol % GO) and 99.2% (5 vol % GO). The Raman spectroscopy data suggested the absence of GO and the formation of multilayer graphene flakes. With increasing graphene content, there was increase in all the measured mechanical parameters: flexural strength (to 1055 ± 64 MPa), Vickers hardness (to 22.76 ± 2.07 GPa), and fracture toughness ($K_{IC}^{5\%GO}$ = 7.32 ± 0.37 MPa $m^{1/2}$). Figure 9 illustrates specific features of crack propagation and indicates crack deflection, pullout of graphene flakes, and bridging with their participation.

In an ideologically congenial work [87], to reach a synergistic effect of the silicon-containing component, SiC whiskers were used, and the GO content of the initial composite powders was increased to 5 and 10 vol %. Hot pressing was carried out as described above [86], and the obtained ceramic samples had somewhat lower densities of 98.5 (5 vol % GO) and 99.3% (10 vol % GO). Increasing graphene content from 5 to 10 vol % led to a decrease both in the flexural strength from 764 to 681 MPa and in the fracture toughness from 6.6 to 5.8 MPa $m^{1/2}$, which was also attributed [87] to the agglomeration of graphene flakes during hot pressing. It was noted that, at a GO content above 20 vol %, the mechanical properties of the produced composite materials were still worse.

Yang et al. [88] indicated peculiarities of the electrostatic interaction in a suspension of graphene oxide

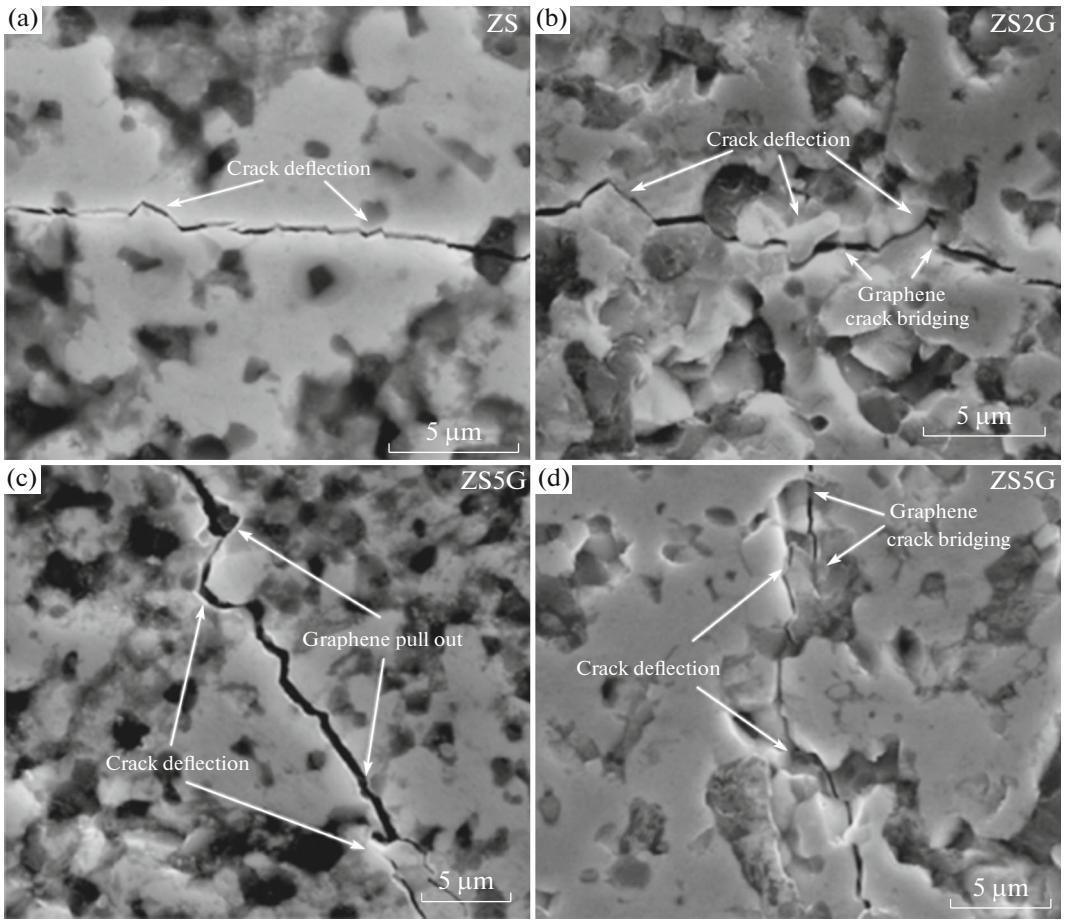

Fig. 9. Crack propagation and crack propagation arrest mechanisms in (a) ZrB_2–SiC material and ZrB_2–SiC–C_G samples containing (b) 2 and (c) 5 vol % GO [86].

particles with ZrB_2 and SiC particles, which have opposite surface charges. This allowed one to obtain more stable dispersions and ensure uniform distribution of components in the bulk of the ZrB_2–20 vol % SiC–(0–3) wt % C_G ceramic materials on their basis. The ceramic composites were produced by SPS at 2000°C (heating rate 100 deg/min, holding time 10 min) and a load of 30 MPa. With increasing graphene content of UHTC from 0.5 to 2 wt %, the flexural strength did not virtually decrease (~1050 → ~940 MPa), and the fracture toughness increased from 5.6 to 6.93 MPa $m^{1/2}$; increasing graphene content to 3 wt % also abruptly decreased both σ_f (~630 MPa) and K_{IC} (4.58 MPa $m^{1/2}$), which may be caused by the formation of aggregates of the carbon components. Moreover, it was noted [88] that the thermal conductivity of the optimal composite containing 2 wt % graphene exceeded that of the unmodified composite by 42%. The combination of the high fracture toughness and the high thermal conductivity led to the fact that the obtained samples had high thermal resistance (Fig. 10, heating to a given temperature and quenching in water); for the ZrB_2–20 vol % SiC–2 wt % C_G sample, $\sigma_f \approx 829$ MPa remains to 500°C.

Thus, the introduction of graphene in the case of its uniform distribution in the bulk of ultra-high-temperature ceramic materials and the absence of significant aggregation enables one to produce materials in which high flexural strength is combined with the good fracture toughness.

2.4. Modification by Short Carbon Fibers

The introduction of short carbon fibers to ultra-high-temperature ceramic composites is an obvious solution for improving the fracture toughness of the latter. Implementation of the concept of the ceramic matrix composites with the corresponding matrix is a technological challenge: depending on the parameters of the C_f skeleton, produced materials are characterized by a clear anisotropy of properties. As reported [89, 90], using short carbon fibers allows one to apply methods that are typically used for producing isotropic ceramic materials.

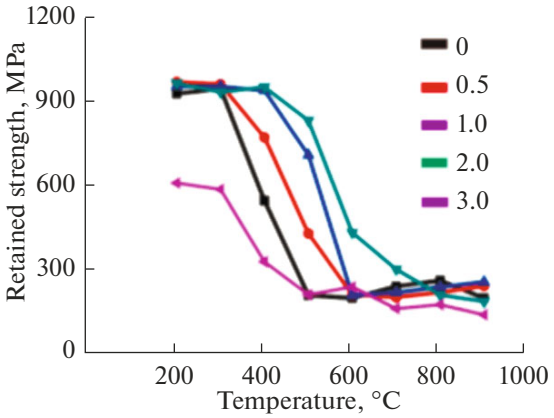

Fig. 10. Residual flexural strength versus temperature for ZrB_2–20 vol % SiC composites containing 0–3 wt % graphene [88].

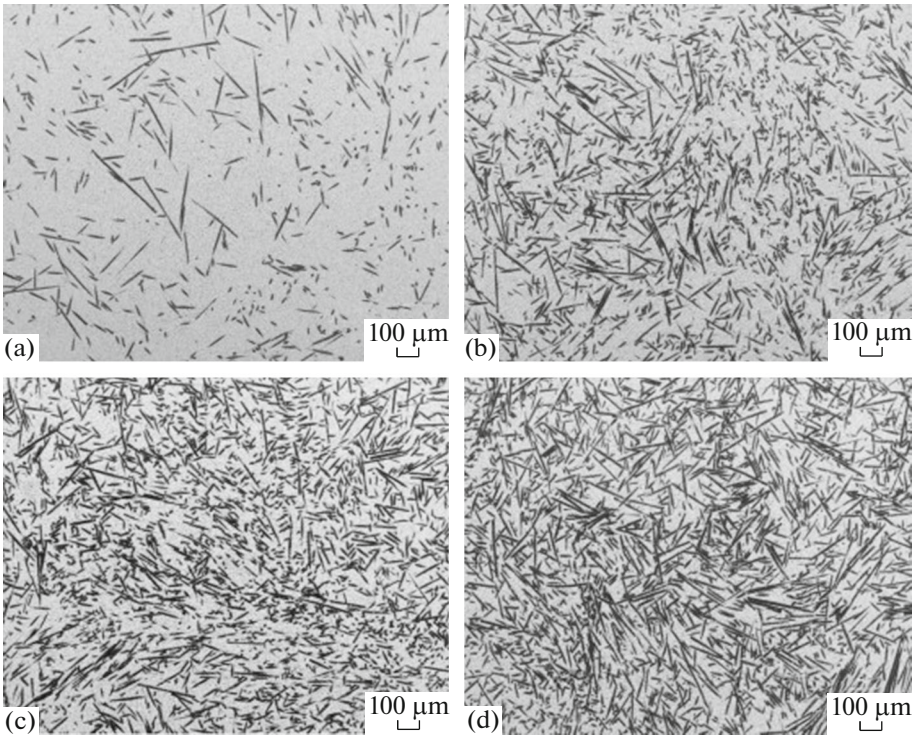

Fig. 11. Microstructures of the polished surfaces of the ZrB_2–20 vol % SiC–x vol % C_f materials at x = (a) 10, (b) 30, (c) 40, and (d) 50 [95].

Yang et al. [89] indicated a 54% increase in the fracture toughness after modification of ZrB_2–20 vol % SiC–20 vol % C_f composite (K_{IC} = 6.56 MPa $m^{1/2}$) synthesized by hot pressing at 2000°C (1 h) and a uniaxial load of 30 MPa. In this synthesis, T800H fibers (Japan) 5 μm in diameter and 2 mm in initial length; after cogrinding of the powders, the fiber length decreased to 200 μm. The flexural strength was 445 ± 36 MPa at a density of the material of 99.3%.

In Guo et al.' [90] and Guo's [91] works, in which the production of samples might probably differ from that in Yang et al.'s study [89] only at the stage of grinding of the initial powders, for materials of a similar composition with a density of 98.5%, somewhat worse values were obtained: σ_f = 397 ± 42 MPa and K_{IC} = 6.35 ± 0.3 MPa $m^{1/2}$. In both cases, the introduction of carbon fibers was noted to decrease the growth of ZrB_2 grains in the producing of ceramic materials. Because of the high hot-pressing tempera-

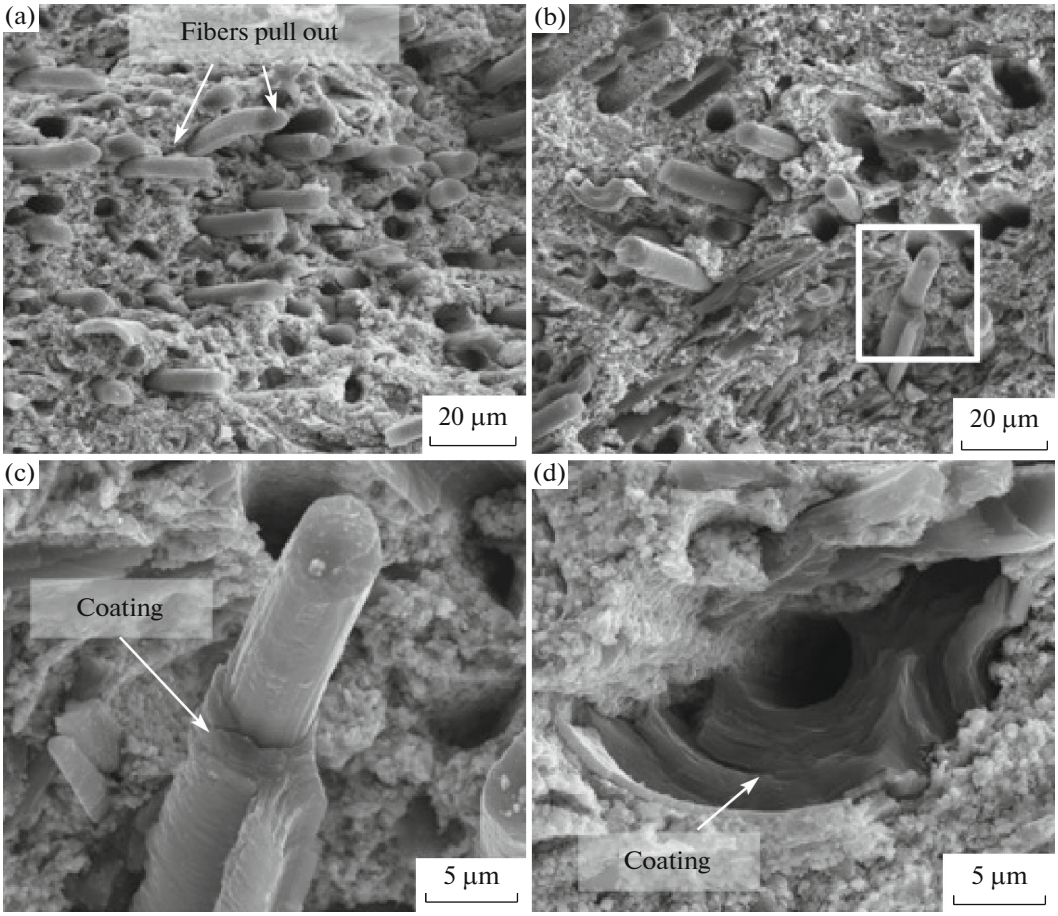

Fig. 12. Microstructures of the surface of a crack in ZrB_2–20 vol % SiC–30 vol % C_f–PyC material [98].

ture (2000°C), not only did a ZrC phase form as the product of the reaction of zirconium dioxide impurity with carbon, but also graphitization of fibers began, which in failure, because of a weak adhesion between the fibers and the matrix, resulted in relatively easy pullout of fibers.

It was shown [92, 93] that the weight loss in the oxidation of the above [89–91] materials both under the conditions of the differential scanning calorimetry in an air flow (to 1500°C) and in the flame of an oxyacetylene torch was somewhat higher than that for the ZrB_2–20 vol % SiC material.

Gui et al. [94] and Hu et al. [95] attempted to obviate the problem of degradation of carbon fibers by graphitization in producing UHTC at the temperature of ~2000°C: they used fibers of another type, XNG-90 pitch-based carbon fibers (Japan), which do not exfoliate at temperatures >1600°C. Gui et al. [94] produced the HfB_2–20 vol % SiC–(20–50) vol % C_f composites by hot pressing (with adding 2 wt % B_4C and 1 wt % C from resin) at the temperature of 2100°C (1 h) and the pressure of 20 MPa. With increasing carbon fiber content of the samples from 20 to 50 vol % [94], there are some decrease in the density from 99.5 to 98.1%, a systematic increase in the fracture toughness from 5.6 to 6.1 MPa $m^{1/2}$, and a virtually linear decrease in the thermal conductivity from 93.8 to 54.4 W/(m K), despite the high thermal conductivity of the introduced fibers. The last fact was explained [94] by the existence of an interphase stress at the fiber–matrix interface. The flexural strength measured at 1600°C for all the composites turned out to be higher than that measured at room temperature: ~340 (1600°C, 20 vol % C_f), ~260 (room temperature, 20 vol % C_f), ~160 (1600°C, 50 vol % C_f), and ~280 (1600°C, 50 vol % C_f).

Hu et al. [95] produced the ZrB_2–20 vol % SiC–(10–50) vol % C_f materials also using pitch-based carbon fibers according to a similar procedure [94] at the lower temperature of 2000°C. As Fig. 11 shows, the distribution of fibers in the bulk of the composites was uniform, and there were no their aggregates. The density of the obtained samples decreased with increasing carbon fiber content of them from 99.8 to 98.1%, and so did the thermal conductivity—from 96 to 48 W/(m K).

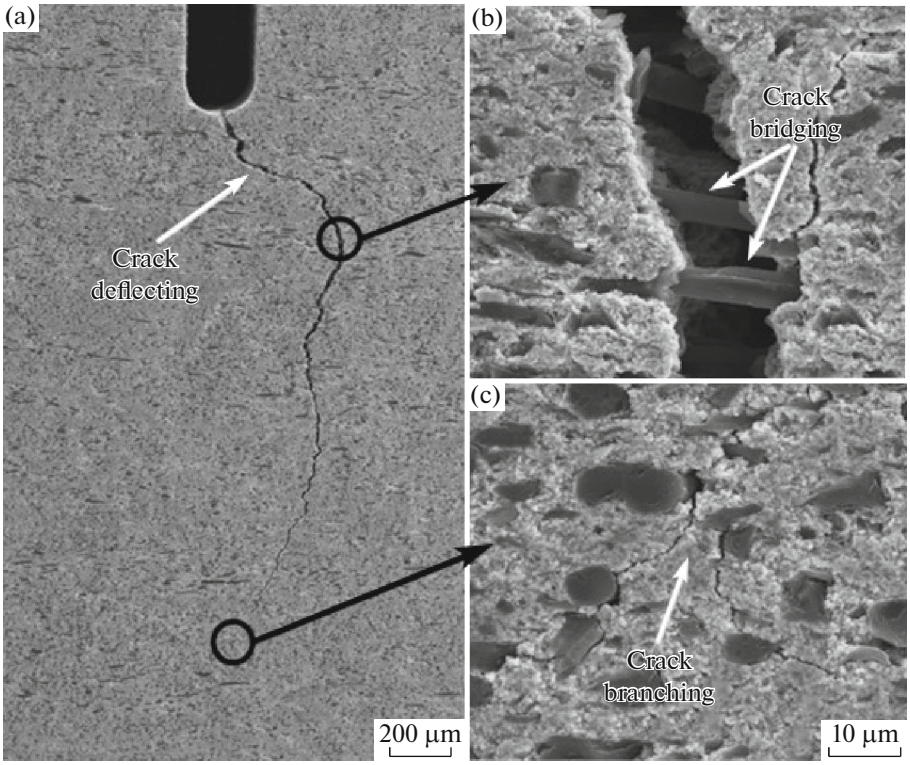

Fig. 13. Crack propagation on the surface of the ZrB_2–20 vol % SiC–30 vol % C_f sample [99].

Hot pressing was also used [96, 97] to explore, by the Taguchi methods, the possibility of obtaining the densest samples [96] and samples with the minimum size of ZrB_2 and SiC grains [97]. It was determined that, within the composition range ZrB_2–(25–15) vol % SiC–(5–15) vol % C_f (C_f were made by Torayca Sigmatex Ltd., UK), the temperature range 1700–1850°C, holding time range 30–90 min, and load range 8–16 MPa, the optimal conditions in both cases were the composition of ZrB_2–20 vol % SiC–10 vol % C_f, the temperature 1850°C, the pressure 16 MPa, and the holding time 30 min.

Shahedi Asl [98] investigated the effect exerted on the mechanical properties of the ZrB_2–20 vol % SiC–30 vol % C_f composites by using nanosized ZrB_2 at the relatively low temperature hot pressing (1600°C to avoid destruction of T800H carbon fibers) and also by the application of a pyrocarbon interphase to fibers. To intensify the densification at low hot-pressing temperature, the process duration was increased to 2 h, with the load being 30 MPa. For the samples in which the fibers were coated with pyrocarbon and in which the fibers were not coated, the relative density was 95–96%, and the flexural strength in the former case was lower (317 MPa) than that in the latter (335 MPa). However, owing to the creation of an interphase, the fracture toughness increased significantly from 4.56 to 6.16 MPa $m^{1/2}$. In failure, there were crack deflection and branching, bridging, and fiber pullout, being particularly characteristic of the ZrB_2–20 vol % SiC–30 vol % C_f–PyC samples (Fig. 12), which were reported [98] to exhibit nonbrittle fracture. The thermal shock resistance determined from the residual strength of the samples after heating and quenching in water for the ZrB_2–20 vol % SiC–30 vol % C_f–PyC samples was higher: ΔT_c increased from 660 to 773°C.

A still lower hot-pressing temperature was used by Balak et al. [99] for the producing ZrB_2–20 vol % SiC–30 vol % C_f materials at 1450°C (2 h, load 30 MPa, Ar). Using nanosized (150 nm) ZrB_2 and finely divided (450 nm) SiC under these conditions resulted in a density of 95.8%, a flexural strength of 341 ± 21 MPa, and a fracture toughness of 6.12 MPa $m^{1/2}$. Nonbrittle fracture of the samples owing to the alignment of the fibers along the C_f-matrix interphase was also detected [99] (Fig. 13). The estimated value of ΔT_c was close to the above value [98] and was 754°C.

Because Balak et al. [99] demonstrated the possibility of producing sufficiently dense composites owing to the use of finely divided initial ZrB_2 and SiC powders, Nasiri et al. [100] considered the effect of the carbon fiber content (from 20 to 50 vol %). Hot pressing was performed similarly [99], but in vacuum (~20 Pa). For the samples containing no more than 30 vol %

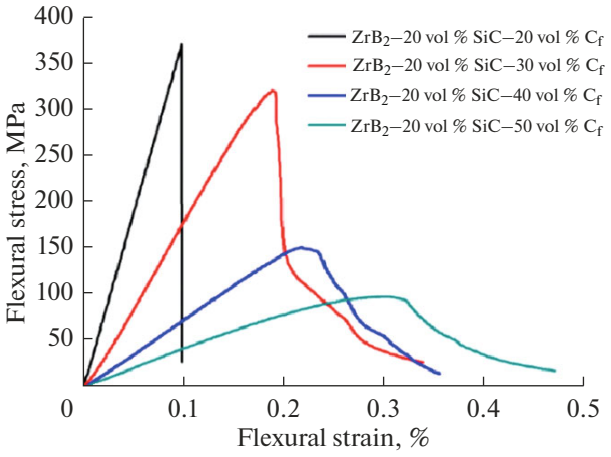

Fig. 14. Flexural deformation of the ZrB_2–SiC–C_f composites with various fiber contents [100].

carbon, the relative density was 97–98%, and with increasing C_f content, it decreased to 80.4% (50 vol % C_f). For the samples containing 20 and 30 vol % C_f, the flexural strengths were 375 and 325 MPa, respectively, and the fracture toughness increased from 5.7 to 5.87 MPa $m^{1/2}$. For the ZrB_2–20 vol % SiC–(20–50) vol % C_f samples, an increasing effect of the reinforcing fibers in failure was observed (Fig. 14).

Tian et al. [101], Shahedi et al. [102], and Lin et al. [103] made the Taguchi analysis of the optimal combinations of process parameters of SPS production of the ZrB_2–SiC UHTC and their composition to reach the best values of fracture toughness [101], hardness [102], and thermal resistance [103]. Tian et al. [101] also analyzed possible additives $MoSi_2$, ZrC, and HfB_2. They determined that the largest contribution to the increase in the fracture toughness was made by an increase in the SHS temperature and the optimization of the SiC content, the addition of ZrC and $MoSi_2$ were of much less importance, and of still lower significance were holding time, C_f content, and time of grinding of the powders. The production of the hardest samples was also maximally affected by an increase in the SPS temperature [102]; for the optimal, in the authors' opinion, the composition ZrB_2–20 vol % SiC–0 vol % C_f of the materials synthesized by SPS at 1850°C (6 min) and 30 MPa, it was found that H_V = 14.8 GPa and K_{IC} = 6.8 MPa $m^{1/2}$. According to Lin et al. [103], the thermal resistance was most influenced by the HfB_2 content, less influenced by the SiC content, and still less influenced by the holding time in SPS. Addition of C_f was reported [103] to have the least influence.

In the conclusion of this section, we should add that Nisar et al. [104] studied the dependence of the main properties (density, hardness, and fracture toughness) on the content of nanosized SiC (~40 nm) and carbon fibers (1.5 μm in diameter) in pressing (200 MPa) with subsequent sintering at 2100 and 2150°C. It was found, that the best characteristics were reached at the SiC_{nano} content of 10 wt %, and increasing C_f content led to a systematic decrease in the hardness. The maximum K_{IC} = 6 MPa $m^{1/2}$ was detected at 10 wt % SiC and 2.5 wt % C_f (2150°C).

In summary, we can say that the introduction of the reinforcing phase of short carbon fibers is a promising way to obviate the problem of brittle fracture of UHTC and significantly increases the thermal resistance. Using high temperatures in hot pressing or spark plasma sintering leads to degradation of the modifying component C_f, which adversely affects the properties of the composite as a whole. Using pitch-based carbon fibers, which are more resistant to high temperature, did not cause fundamental improvement of the properties. To reduce the sintering temperature, it was proposed to use the nanodispersed components ZrB_2/HfB_2 and SiC, but this may be the cause of the emergence of zirconium or hafnium oxide impurity.

It should also be noted that using carbon fibers about several micrometers in diameter may lead to significant impairment of the oxidation resistance of UHTC, particularly at high fiber contents.

2.5. Modification by Carbon Nanotubes

Nisar et al.'s work [105] was the one of the first studies of the introduction of carbon nanotubes (CNT) to UHTC. For this purpose, CNT (d = 10–20 nm) were ultrasonically dispersed in the butanol with subsequent addition of ZrB_2 and SiC powders in the ratio ZrB_2–20 vol % SiC–2 wt % C_{CNT}; the powder obtained after drying and grinding was hot-pressed at 1900°C (1 h) and a load of 30 MPa. The flexural strength of the obtained samples was 616 ± 97 MPa, the hardness was 15.5 ± 0.9 GPa, and the fracture toughness only slightly (~15%) exceeded that of the unmodified samples [101]. Such the results were explained [105] by too strong binding between the nanotubes and the ceramic matrix and by destruction of CNT during high-temperature compaction.

Nisar and Balani [106] showed that, in producing the ZrB_2–20 vol % SiC–10 vol % C_{CNT} material, the nanotubes are agglomerated primarily on the surface of SiC particles, thus preventing oxide impurities from being removed from the surface of ZrB_2 in hot pressing (1850°C, 1 h, 20 MPa). It was stated [106] that the elevated fracture toughness (K_{IC} = 5.1 ± 0.8 MPa $m^{1/2}$ at a density of 93.8%) of this material was due to manifold crack deflections at grain boundary and also to possible pullout of the nanotubes in failure (Fig. 15).

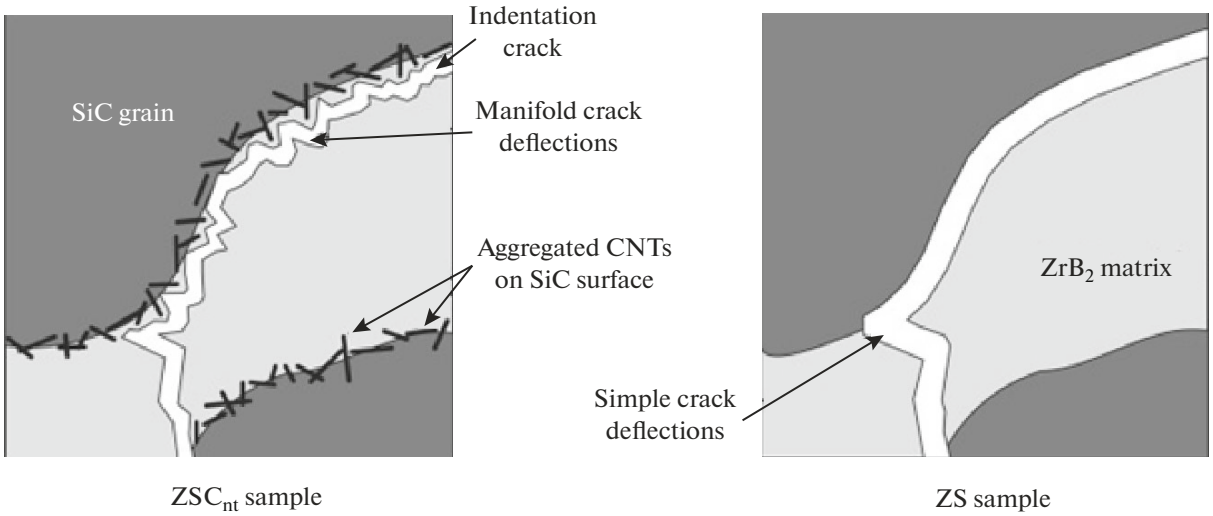

Fig. 15. Schematic representation of the path of a crack along the boundary of a SiC grain in the ZrB_2–SiC composites reinforced and unreinforced with CNT [106].

Spark plasma sintering was also used for obtaining CNT-modified composites based on MB_2–SiC [107–110]. A study was made of the effect of the process temperature on the mechanical properties of ZrB_2–20 vol % SiC–15 vol % C_{CNT} at constant holding time (10 min) and constant load (25 MPa) [107]. With increasing SPS temperature from 1600 to 1750°C, there are both densification (the density increased from 94.6 to 99.1%) and an increase in σ_f (472 → 565 MPa), H_V (11.5 → 16.0 GPa), and K_{IC} (5.9 → 8.0 MPa $m^{1/2}$), and in the process at 1800°C, the density remains unchanged, and all the other quantities considerably decreased, which was ascribed [107] to an abrupt increase in the ZrB_2 grain size from 2.0 (1750°C) to 3.4 μm (1800°C).

Zhang et al. [108] and An et al. [109] produced the ZrB_2–20 vol % SiC–10 vol % C_{CNT} ceramic materials by SPS using stepwise heating 1300 → 1500 → 1650°C with holding for 5 min at each step (heating rate 150 deg/min, load 40 MPa, Ar). In this case, the density was 99.7%, which was likely to be the cause of the fact that the flexural strength of the CNT-modified composite (390.4 MPa) exceeded that of the ZrB_2–20 vol % SiC ceramic obtained under similar conditions. The high $K_{IC} = 9.5 \pm 0.8$ MPa $m^{1/2}$ was assigned [108] to a decrease in the residual interphase stresses between the matrix and the reinforcing filler, which was ensured by the chosen pressing method. Figure 16 illustrates the authors' concepts of the synergistic effect on the fracture toughness owing to the simultaneous presence of the silicon carbide particles and carbon nanotubes.

Exposure of the surface of the ZrB_2–20 vol % SiC–10 vol % C_{CNT} samples for 30 s to an air flow (heat flux 2.5 MW/m^2, T_{max} = 2750°C) using a plasma arc jet did not change the appearance, and the carbon nanotubes were found (by Raman spectroscopy) to be present both in the unoxidized region and in the oxidized layer consisting primarily of ZrO_2 and SiO_2 [109]. An elevated high-temperature thermal conductivity of the obtained material of the ZrB_2–20 vol % SiC–10 vol % C_{CNT} was noted. This manifested itself in the fact that the temperature of the opposite part of the sample during the test for this material was the higher than that for ZrB_2–20 vol % SiC.

The interesting data were published on the synthesis and properties of 37 vol % ZrB_2–37 vol % HfB_2–20 vol % SiC–6 vol % C_{CNT} composite material [110]. By SPS in vacuum (1850°C, holding time 10 min, 30 MPa), the samples with a density of 99.5% were obtained. The hardness of the material was 28.1 GPa, and the fracture toughness was 10.2 MPa $m^{1/2}$. According to the X-ray powder diffraction data, the SPS conditions turned out to be sufficient for the solid solution ZrB_2–HfB_2 to form. Such significant improvement of the properties was attributed [110] to the fact that the addition of two modifying phases (SiC and CNT) generated interphase stresses (compressive for the reinforcing component and tensile for the matrix). We consider it possible that this was the implementation of the beneficial properties of the formed solid solution ZrB_2–HfB_2 as a certain prototype of high-entropy materials.

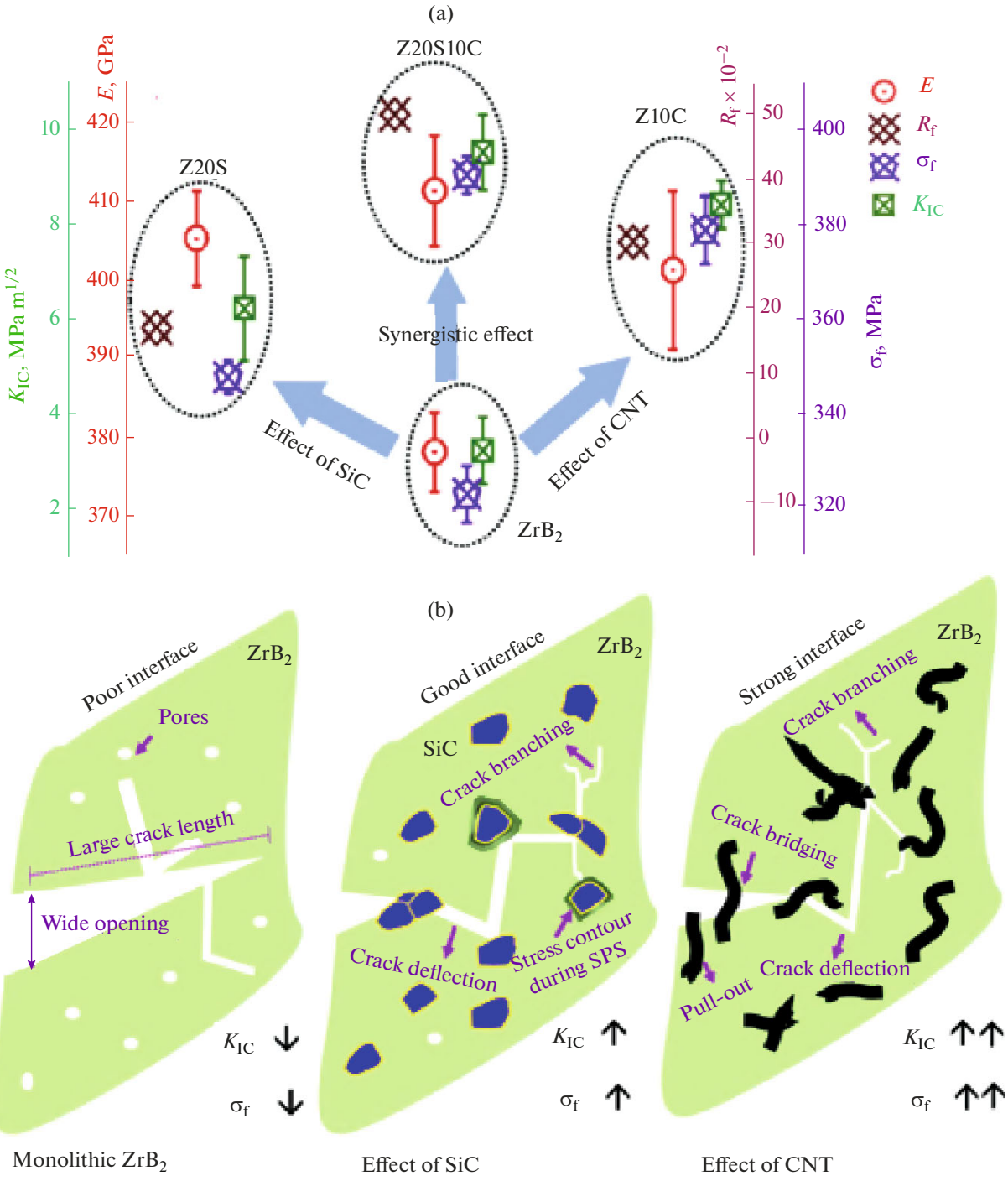

Fig. 16. (a) Overall diagram of mechanical properties and (b) scheme of the mechanism of toughening in ZrB_2–SiC–CNT UHTC [108].

By and large, we can state that the modification of the bulk of UHTC by the carbon nanotubes significantly increases the fracture toughness of materials (to K_{IC} = 8–10 MPa $m^{1/2}$); however, the process of production of such ceramic composites requires a conscious choice of the hot-pressing temperature and the maximum dispersion of CNT.

CONCLUSION

Having analyzed the above data, we can make several general conclusions.

(1) Data on the processes of oxidation of UHTC modified by carbon components (probably, except carbon fibers) are within the general concepts of oxidation of the ZrB_2/HfB_2–SiC materials: the oxidation

gives rise to a multilayer structure, and the compositions of the individual layers are determined by temperature and oxygen pressure. Introduction of carbon materials to ceramic composite does not prevent processes of active oxidation of SiC under the borosilicate glass layer.

(2) The method of cold pressing with subsequent sintering without loading, which could have significantly simplified the production of UHTC and improved its productivity, has not yet allowed one to approach the mechanical properties of samples obtained by hot pressing or spark plasma sintering, even with introducing carbon components as sintering additives. Using the nanosized powders, in particular SiC, in combination with reinforcing by short carbon fibers somewhat increases the fracture toughness, but the porosity cannot be decreased below 3–4%.

(3) All the considered carbon components can significantly (severalfold) inhibit the ZrB_2 grain growth, which improves the fracture toughness and the thermal shock resistance.

(4) Modification of the ZrB_2/HfB_2–SiC materials by amorphous carbon, graphite, and graphene increases the thermal conductivity over a wide range of the temperatures of the ceramic composites generally owing to the improvement of heat transfer routes, whereas addition of equally the high-thermal-conductivity short carbon fibers decreases the thermal conductivity of MB_2–SiC–C material, probably, because of the generation of an interphase stress at the fiber–matrix interface. The effect exerted on the thermal conductivity of UHTC by the application of the interphase on the surface of a reinforcing fiber is not described in the literature.

(5) Increasing carbon component content of ultra-high-temperature ceramic material decreases the flexural strength. A certain exception is graphene-modified materials, for which, up to some graphene content, the decrease in σ_f is not so significant.

(6) Not only can oxidation processes on the surface of the MB_2–SiC–C materials influence their further oxidation behavior, but also they can change their mechanical properties, either because of healing surface defects by the borosilicate glass (temperature below 1700–1800°C, relatively high oxygen pressure) or because of the formation of a porous, brittle, and readily detachable layer based on the ZrO_2/HfO_2 on the surface (high temperatures, low oxygen pressures).

Thus, we can conclude that introduction of the carbon components, especially carbon fibers, nanotubes, and graphene, improves the mechanical properties of UHTC. However, to date, by no means all of the problems have been successfully solved; therefore, the reviewed area of research is quite promising and practically important.

ACKNOWLEDGMENTS

This work was supported by the Council for Grants of the President of the Russian Federation (grant no. MD-5535.2018.3).

REFERENCES

1. G. V. Samsonov, *Refractory Compounds: A Handbook of Properties and Applications* (Metallurgizdat, Moscow, 1963). [in Russian]
2. P. Rogl and P. E. Potter, Calphad **12**, 191 (1988). doi 10.1016/0364-5916(88)90021-1
3. R. Rogl and H. Bittermann, J. Solid State Chem. **154**, 257 (2000). doi 10.1006/jssc.2000.8846
4. E. Rudy and S. Windisch, *Report AFML-TR-65–2* (Air Force Materials Laboratory, Wright Patterson Air Force Base, Ohio, 1966), Part II, Vol. XIII, pp. 1–212.
5. K. P. Portnoi, V. M. Romashov, and L. I. Vyroshina, Poroshk. Metall. **91** (7), 68 (1970).
6. G. V. Samsonov, A. S. Bolgar, E. A. Guseva, et al., High Temp.–High Pressures **5**, 29 (1973).
7. G. V. Samsonov and L. Ya. Markovskii, Usp. Khim. **XXV**, 190 (1956).
8. P. Schwarzkopf and R. Kieffer, *Refractory Hard Metals: Borides, Carbides, Nitrides, and Silicides: the Basic Constituents of Cemented Hard Metals and Their Use as High-Temperature Materials* (Macmillan, New York, 1953).
9. E. P. Simonenko, D. V. Sevast'yanov, N. P. Simonenko, et al., Russ. J. Inorg. Chem. **58**, 1669 (2013). doi 10.1134/S0036023613140039
10. R. Savino, L. Criscuolo, G. D. Di Martino, and S. Mungiguerra, J. Eur. Ceram. Soc. **38**, 2937 (2018). doi 10.1016/j.jeurceramsoc.2017.12.043
11. A. Paul, J. Binner, and B. Vaidhyanathan, in *Ultra-High Temperature Ceramics: Materials for Extreme Environment Applications*, Ed. by W. G. Fahrenholtz, E. J. Wuchina, W. E. Lee, and Y. Zhou (Wiley-Blackwell, New York, 2014), pp. 144–166. doi 10.1002/9781118700853.ch7
12. L. Silvestroni, H.-J. Kleebe, W. G. Fahrenholtz, and J. Watts, Sci. Rep. **7**, Article no. 40730 (2017). doi 10.1038/srep40730
13. S. Guo, J. Am. Ceram. Soc. **101**, 2707 (2018). doi 10.1111/jace.15446
14. E. Zapata-Solvas, D. Gomez-Garcia, A. Dominguez-Rodriguez, and W. E. Lee, J. Eur. Ceram. Soc. **38**, 47 (2017). doi 10.1016/j.jeurceramsoc.2017.08.028
15. W. G. Fahrenholtz and G. E. Hilmas, Scripta Mater. **129**, 94 (2017). doi 10.1016/j.scriptamat.2016.10.018
16. E. P. Simonenko, N. P. Simonenko, A. N. Gordeev, et al., Russ. J. Inorg. Chem. **63**, 421 (2018). doi 10.1134/S0036023618040186
17. F. Monteverde and R. Savino, J. Am. Ceram. Soc. **95**, 2282 (2012). doi 10.1111/j.1551-2916.2012.05226.x
18. X. Jin, R. He, X. Zhang, P. Hu, J. Alloys Compd. **566**, 125 (2013). doi 10.1016/j.jallcom.2013.03.067
19. F. Monteverde and R. Savino, J. Am. Ceram. Soc. **95**, 2282 (2012). doi 10.1111/j.1551-2916.2012.05226.x

20. A. Cecere, R. Savino, C. Allouis, and F. Monteverde, Int. J. Heat Mass Transfer **91**, 747 (2015). doi 10.1016/j.ijheatmasstransfer.2015.08.029
21. T. A. Parthasarathy, M. D. Petry, M. K. Cinibulk, et al., J. Am. Ceram. Soc. **96**, 907 (2013). doi 10.1111/jace.12180
22. T. H. Squire and J. Marschall, J. Eur. Ceram. Soc. **30**, 2239 (2010).
23. V. G. Sevastyanov, E. P. Simonenko, A. N. Gordeev, et al., Russ. J. Inorg. Chem. **59**, 1298 (2014). doi 10.1134/S0036023614110217
24. V. G. Sevastyanov, E. P. Simonenko, A. N. Gordeev, et al., Russ. J. Inorg. Chem. **60**, 1360 (2015). doi 10.1134/S0036023615110133
25. E. P. Simonenko, A. N. Gordeev, N. P. Simonenko, et al., Russ. J. Inorg. Chem. **61**, 1203 (2016). doi 10.1134/S003602361610017X
26. V. G. Sevast'yanov, E. P. Simonenko, A. N. Gordeev, et al., Russ. J. Inorg. Chem. **58**, 1269 (2013). doi 10.1134/S003602361311017X
27. V. G. Sevastyanov, E. P. Simonenko, A. N. Gordeev, et al., Russ. J. Inorg. Chem. **59**, 1361 (2014). doi 10.1134/S0036023614120250
28. Yu. B. Lyamin, V. Z. Poilov, E. N. Pryamilova, et al., Russ. J. Inorg. Chem. **61**, 149 (2016). doi 10.1134/S0036023616020133
29. D. V. Grashchenkov, O. Yu. Sorokin, Yu. E. Lebedeva, and M. L. Vaganova, Russ. J. Appl. Chem. **88**, 386 (2015).
30. P. S. Sokolov, A. V. Arakcheev, I. L. Mikhal'chik, et al., Refract. Ind. Ceram. **58**, 46 (2017). doi 10.1007/s11148-017-0052-9
31. L. A. Chevykalova, I. Yu. Kelina, I. L. Mikhal'chik, et al., Refract. Ind. Ceram. **54**, 455 (2014).
32. D. V. Kolovertnov and I. B. Ban'kovskaya, Glass Phys. Chem. **41**, 324 (2015).
33. C. Wei, S. Li, K. Yin, et al., Ceram. Int. **44**, 4385 (2018). doi 10.1016/j.ceramint.2017.12.036
34. S. Guo, J. Ceram. Soc. Jpn. **124**, 166 (2016). doi 10.2109/jcersj2.15190
35. C. Wei and C. Ye, Int. J. Refract. Met. Hard Mater. **51**, 233 (2015). doi 10.1016/j.ijrmhm.2015.04.023
36. L.-L. Wang, J. Liang, G.-D. Fang, et al., Ceram. Int. **40**, 5255 (2014). doi 10.1016/j.ceramint.2013.10.097
37. C. Wei, X. Zhang, and S. Li, Ceram. Int. **40**, 5001 (2014). doi 10.1016/j.ceramint.2013.08.070
38. M. M. Opeka, I. G. Talmy, and J. A. Zaykoski, J. Mater. Sci. **39**, 5887 (2004). doi 10.1023/B:JMSC.0000041686.21788.77
39. J. Han, P. Hu, X. Zhang, et al., Compos. Sci. Technol. **68**, 799 (2008). doi 10.1016/j.compscitech.2007.08.017
40. T. A. Parthasarathy, R. A. Rapp, M. Opeka, and M. K. Cinibulk, J. Am. Ceram. Soc. **95**, 338 (2012). doi 10.1111/j.1551-2916.2011.04927.x
41. E. Eakins, D. D. Jayaseelan, and W. E. Lee, Metall. Mater. Trans. A. **42A**, 878 (2011). doi 10.1007/s11661-010-0540-8
42. D. Gao, Y. Zhang, J. Fu, et al., Corros. Sci. **52**, 3297 (2010). doi 10.1016/j.corsci.2010.06.004
43. K. S. Cissel and E. Opila, J. Am. Ceram. Soc. **101**, 1765 (2018). doi 10.1111/jace.15298
44. W. G. Fahrenholtz, J. Am. Ceram. Soc. **90**, 143 (2007). doi 10.1111/j.1551-2916.2006.01329.x
45. J. Li, T. J. Lenosky, C. J. Foörst, and S. Yip, J. Am. Ceram. Soc. **91**, 1475 (2008). doi 10.1111/j.1551-2916.2008.02319.x
46. A. Rezaie, W. G. Fahrenholtz, and G. E. Hilmas, J. Eur. Ceram. Soc. **33**, 413 (2013). doi 10.1016/j.jeurceramsoc.2012.09.016
47. H. Jin, S. Meng, X. Zhang, et al., J. Am. Ceram. Soc. **99**, 2474 (2016). doi 10.1111/jace.14232
48. Q. N. Nguyen, E. J. Opila, and R. C. Robinson, J. Electrochem. Soc. **151**, B558 (2004). doi 10.1149/1.1786929
49. C.-L. Zhou, Y.-Y. Wang, Z.-Q. Cheng, et al., Adv. Mat. Res. **105–106**, 199 (2010). doi 10.4028/www.scientific.net/AMR.105-106.199
50. H. Zhang, Y. Yan, Z. Huang, et al., J. Am. Ceram. Soc. **92**, 1599 (2009). doi 10.1111/j.1551-2916.2009.03039.x
51. X.-J. Zhou, G.-J. Zhang, Y.-G. Li, et al., Mater. Lett. **61**, 960 (2007). doi 10.1016/j.matlet.2006.06.024
52. S. Zhou, Z. Wang, X. Sun, and J. Han, Mater. Chem. Phys. **122**, 470 (2010). doi 10.1016/j.matchemphys.2010.03.028
53. X. Sun, X. Zhang, Z. Wang, et al., Key Eng. Mater. **434–435**, 185 (2010). doi 10.4028/www.scientific.net/KEM.434-435.185
54. W.-M. Guo, Y. You, G.-J. Zhang, et al., J. Eur. Ceram. Soc. **35**, 1985 (2015). doi 10.1016/j.jeurceramsoc.2014.12.026
55. X. Zhang, Z. Wang, X. Sun, et al., Mater. Lett. **62**, 4360 (2008). doi 10.1016/j.matlet.2008.07.027
56. Z. Wang, S. Wang, X. Zhang, et al., J. Alloys Compd. **484**, 390 (2009). doi 10.1016/j.jallcom.2009.04.109
57. H. Jin, S. Meng, Q. Yang, and Y. Zhu, Ceram. Int. **39**, 5591 (2013). doi 10.1016/j.ceramint.2012.12.074
58. H. Jin, S. Meng, Y. Zhu, and Y. Zhou, Mater. Des. **50**, 509 (2013). doi 10.1016/j.matdes.2013.03.025
59. H. Jin, S. Meng, Q. Yang, and Y. Zhu, Ceram. Int. **39**, 5591 (2013). doi 10.1016/j.ceramint.2012.12.074
60. X. H. Zhang, Z. Wang, P. Hu, et al., Scripta Mater. **61**, 809 (2009). doi 10.1016/j.scriptamat.2009.07.001
61. Z. Wang, C. Hong, X. Zhang, et al., Mater. Chem. Phys. **113**, 338 (2009). doi 10.1016/j.matchemphys.2008.07.095
62. S. Zhou, Z. Wang, and W. Zhang, J. Alloys Compd. **485**, 181 (2009). doi 10.1016/j.jallcom.2009.05.126
63. P. Hu, Z. Wang, and X. Sun, Int. J. Refract. Met. Hard Mater. **28**, 280 (2010). doi 10.1016/j.ijrmhm.2009.10.013
64. Z. Wang, Q. Qu, Z. Wu, and G. Shi, J. Alloys Compd. **509**, 6871 (2011). doi 10.1016/j.jallcom.2011.03.163
65. L. Wang, J. Liang, and G. Fang, J. Alloys Compd. **619**, 145 (2015). doi 10.1016/j.jallcom.2014.08.255
66. J. Niu, H. Jin, S. Meng, et al., Ceram. Int. **42**, 5562 (2016). doi 10.1016/j.ceramint.2015.12.031

67. H. Jin, S. Meng, X. Zhang, et al., J. Eur. Ceram. Soc. **36**, 1855 (2016). doi 10.1016/j.jeurceramsoc.2016.02.040
68. Z. Wang, Z. Wu, and G. Shi, Mater. Sci. Eng., A. **A528**, 2870 (2011). doi 10.1016/j.msea.2010.12.079
69. L. Wang, D. Kong, G. Fang, and J. Liang, Int. J. Appl. Ceram. Technol. **14**, 31 (2017). doi 10.1111/ijac.12613
70. R. Zhang, X. Cheng, D. Fang, et al., Mater. Des. **52**, 17 (2013). doi 10.1016/j.matdes.2013.05.045
71. X. Chen, X. Peng, Z. Wei, et al., Mater. Des. **126**, 91 (2017). doi 10.1016/j.matdes.2017.04.001
72. X. Zhang, Z. Wang, X. Sun, et al., Int. J. Mod. Phys. B **23**, 1160 (2009). doi 10.1142/S0217979209060622
73. V. Zamora, M. Nygren, F. Guiberteau, and A. L. Ortiz, Ceram. Int. **40**, 11457 (2014). doi 10.1016/j.ceramint.2014.03.130
74. M. Shahedi Asl, M. J. Zamharir, Z. Ahmadi, and S. Parvizi, Mater. Sci. Eng., A **716**, 99 (2018). doi 10.1016/j.msea.2018.01.038
75. M. Shahedi Asl, Ceram. Int. **44**, 6935 (2018). doi 10.1016/j.ceramint.2018.01.122
76. Y. H. Cheng, Y. Qi, P. Hu, et al., J. Am. Ceram. Soc. **99**, 2131 (2016). doi 10.1111/jace.14192
77. E. P. Simonenko, N. P. Simonenko, V. G. Sevastyanov, and N. T. Kuznetsov, Russ. J. Inorg. Chem. **61**, 1483 (2016). doi 10.1134/S0036023616120172
78. E. P. Simonenko, N. P. Simonenko, D. V. Sevastyanov, et al., Russ. J. Inorg. Chem. **61**, 1649 (2016). doi 10.1134/S0036023616130039
79. F. Li, Y. Cao, J. Liu, et al., Ceram. Int. **43**, 7743 (2017). doi 10.1016/j.ceramint.2017.03.080
80. Y. Cao, H. Zhang, F. Li, et al., Ceram. Int. **41**, 7823 (2015). doi 10.1016/j.ceramint.2015.02.117
81. E. P. Simonenko, N. P. Simonenko, E. K. Papynov, et al. Russ. J. Inorg. Chem. **63**, 1 (2018). doi 10.1134/S0036023618010187
82. N. T. Kuznetsov, V. G. Sevastyanov, E. P. Simonenko, and N. P. Simonenko, RU Patent No. 2618567, 04.05.2017.
83. E. P. Simonenko, N. P. Simonenko, A. N. Gordeev, et al., Russ. J. Inorg. Chem. **63**, 1345, (2018) doi 10.1134/S0036023618100170
84. E. P. Simonenko, N. P. Simonenko, A. N. Gordeev, et al., Russ. J. Inorg. Chem. **63**, 1484, (2018) doi 10.1134/S0036023618110177
85. F. Yang, X. Zhang, J. Han, and S. Du, Mater. Lett. **62**, 2925 (2008). doi 10.1016/j.matlet.2008.01.076
86. F. Yang, X. Zhang, J. Han, and S. Du, Mater. Des. **29**, 1817 (2008). doi 10.1016/j.matdes.2008.03.011
87. F. Yang, X. Zhang, J. Han, and S. Diu, J. Compos. Mater. **44**, 953 (2010). doi 10.1177/0021998309346545
88. F.-Y. Yang, X.-H. Zhang, and S.-Y. Du, Key Eng. Mater. **368–372**, 1753 (2008). doi 10.4028/www.scientific.net/KEM.368-372.1753
89. F. Yang, X. Zhang, J. Han, and S. Du, J. Alloys Compd. **472**, 395 (2009). doi 10.1016/j.jallcom.2008.04.092
90. S. Guo, K. Naito, and Y. Kagawa, Ceram. Int. **39**, 1567 (2013). doi 10.1016/j.ceramint.2012.07.108
91. S. Guo, Ceram. Int. **39**, 5733 (2013). doi 10.1016/j.ceramint.2012.12.091
92. M. Shahedi Asl, F. Golmohammadi, M. Ghassemi Kakroudi, and M. Shokouhimehr, Ceram. Int. **42**, 4498 (2016). doi 10.1016/j.ceramint.2015.11.139
93. M. Shahedi Asl, M. G. Kakroudi, I. Farahbakhsh, et al., Ceram. Int. **42**, 18612 (2016). doi 10.1016/j.ceramint.2016.08.205
94. K. Gui, P. Hu, W. Hong, et al., J. Alloys Compd. **706**, 16 (2017). doi 10.1016/j.jallcom.2017.02.227
95. P. Hu, K. Gui, W. Hong, et al., J. Eur. Ceram. Soc. **37**, 2317 (2017). doi 10.1016/j.jeurceramsoc.2017.02.008
96. W. Hong, K. Gui, P. Gui, et al., J. Adv. Ceram. **6**, 110 (2017). doi 10.1007/s40145-017-0223-7
97. Z. Balak, M. Shahedi Asl, M. Azizieh, et al., Ceram. Int. **43**, 2209 (2017). doi 10.1016/j.ceramint.2016.11.005
98. M. Shahedi Asl, Ceram. Int. **43**, 15047 (2017). doi 10.1016/j.ceramint.2017.08.030
99. Z. Balak, M. Azizieh, H. Kafashan, et al., Mater. Chem. Phys. **196**, 333 (2017). doi 10.1016/j.matchemphys.2017.04.062
100. Z. Nasiri, M. Mashhadi, and A. Abdollahi, Int. J. Refract. Met. Hard Mater. **51**, 216 (2015). doi 10.1016/j.ijrmhm.2015.04.005
101. W.-B. Tian, Y.-M. Kan, G.-J. Zhang, et al., Mater. Sci. Eng., A **A487**, 568 (2008). doi 10.1016/j.msea.2007.11.027
102. M. Shahedi Asl, I. Farahbakhsh, and B. Nayebi, Ceram. Int. **42**, 1950 (2016). doi 10.1016/j.ceramint.2015.09.165
103. J. Lin, Y. Huang, H. Zhang, et al., Ceram. Int. **41**, 15261 (2015). doi 10.1016/j.ceramint.2015.07.207
104. A. Nisar, S. Ariharan, and K. Balani, Ceram. Int. **43**, 13483 (2017). doi 10.1016/j.ceramint.2017.07.053
105. A. Nisar, S. Ariharan, T. Venkateswaran, et al., Carbon **111**, 269 (2017). doi 10.1016/j.carbon.2016.10.002
106. A. Nisar and K. Balani, Coatings **7**, 110/1 (2017). doi 10.3390/coatings7080110
107. M. Shahedi Asl and M. Ghassemi Kakroudi, Mater. Sci. Eng., A. **625**, 385 (2015). doi 10.1016/j.msea.2014.12.028
108. X. Zhang, Y. An, J. Han, et al., RSC Adv. **5**, 47060 (2015). doi 10.1039/C5RA05922D
109. Y. An, X. Xu, and K. Gui, Ceram. Int. **42**, 14066 (2016). doi 10.1016/j.ceramint.2016.06.014
110. B. Zhang, X. Zhang, C. Hong, et al., ACS Appl. Mater. Interfaces **8**, 11675 (2016). doi 10.1021/acsami.6b00822

Translated by V. Glyanchenko